Journal of Hydrology 561 (2018) 59–75

Contents lists available at ScienceDirect

Journal of Hydrology

journal homepage: www.elsevier.com/locate/jhydrol

Research papers

Evaporation from a temperate closed-basin lake and its impact on present, past, and future water level

Ke Xiao[a,*], Timothy J. Griffis[a], John M. Baker[a,b], Paul V. Bolstad[c], Matt D. Erickson[a], Xuhui Lee[d,e], Jeffrey D. Wood[a,f], Cheng Hu[e], John L. Nieber[g]

[a] Department of Soil, Water, and Climate, University of Minnesota, Twin Cities, Saint Paul, MN, USA
[b] USDA-ARS Soil and Water Research Unit, Saint Paul, MN, USA
[c] Department of Forest Resources, University of Minnesota, Twin Cities, Saint Paul, MN, USA
[d] School of Forestry and Environmental Studies, Yale University, New Haven, CT, USA
[e] Yale-NUIST Center on Atmospheric Environment, Nanjing University of Information Science and Technology, Nanjing, Jiangsu, China
[f] School of Natural Resources, University of Missouri, Columbia, MO, USA
[g] Department of Bioproducts and Biosystems Engineering, University of Minnesota, Twin Cities, Saint Paul, MN, USA

ARTICLE INFO

This manuscript was handled by Tim R. McVicar, Editor-in-Chief, with the assistance of Joshua Larsen, Associate Editor

Keywords:
Evaporation
Lake
Eddy covariance
Modeling
Ice phenology
Water level

ABSTRACT

Lakes provide enormous economic, recreational, and aesthetic benefits to citizens. These ecosystem services may be adversely impacted by climate change. In the Twin Cities Metropolitan Area of Minnesota, USA, many lakes have been at historic low levels and water augmentation strategies have been proposed to alleviate the problem. White Bear Lake (WBL) is a notable example. Its water level declined 1.5 m during 2003–2013 for reasons that are not fully understood. This study examined current, past, and future lake evaporation to better understand how climate will impact the water balance of lakes within this region. Evaporation from WBL was measured from July 2014 to February 2017 using two eddy covariance (EC) systems to provide better constraints on the water budget and to investigate the impact of evaporation on lake level. The estimated annual evaporation losses for years 2014 through 2016 were 559 ± 22 mm, 779 ± 81 mm, and 766 ± 11 mm, respectively. The higher evaporation in 2015 and 2016 was caused by the combined effects of larger average daily evaporation and a longer ice-free season. The EC measurements were used to tune the Community Land Model 4 – Lake, Ice, Snow and Sediment Simulator (CLM4-LISSS) to estimate lake evaporation over the period 1979–2016. Retrospective analyses indicate that WBL evaporation increased during this time by about 3.8 mm year^{-1}, which was driven by increased wind speed and lake-surface vapor pressure gradient. Using a business-as-usual greenhouse gas emission scenario (RCP8.5), lake evaporation was modeled forward in time from 2017 to 2100. Annual evaporation is expected to increase by 1.4 mm year^{-1} over this century, largely driven by lengthening ice-free periods. These changes in ice phenology and evaporation will have important implications for the regional water balance, and water management and water augmentation strategies that are being proposed for these Metropolitan lakes.

1. Introduction

The physical aspects of temperate closed-basin lakes, such as water level, water temperature, and ice phenology, are highly sensitive to variations in climate (Adrian et al., 2009; Schindler 2009). Since their contributing watersheds are often relatively small, streamflow is typically a minor component of their water balance, which is primarily controlled by precipitation, evaporation, and groundwater exchange (Almendinger, 1990; Winter, 1995). Short-term water level change of closed-basin lakes is most influenced by changes in precipitation and evaporation (van der Kamp et al., 2008), while the interaction with groundwater tends to impact lake water level at longer time scales and acts to dampen seasonal and inter-annual lake level changes (Kirillin et al., 2013). In general, the water levels of closed-basin lakes are subject to larger variations than flow-through lakes, and in some cases, water level can vary several meters within a decade (e.g. Almendinger, 1990; Ayenew and Becht, 2008). Attribution of the cause(s) of such changes is challenging, since the only data typically available are precipitation records.

Evaporation is the major sink (loss) term in the lake water budget of

* Corresponding author at: 439 Borlaug Hall, 1991 Upper Buford Circle, Saint Paul, MN 55108, USA.
E-mail address: xiaox224@umn.edu (K. Xiao).

https://doi.org/10.1016/j.jhydrol.2018.03.059
Received 19 May 2017; Received in revised form 17 March 2018; Accepted 21 March 2018
Available online 22 March 2018
0022-1694/ © 2018 Elsevier B.V. All rights reserved.

temperate closed-basin lakes. Better constraints on lake evaporation are needed to improve our understanding of present, past, and future changes in water levels. Key results of relevant studies on lake evaporation and water budgets for closed-basin lakes are summarized in Table 1. In most of these studies, lake evaporation has been estimated using indirect methods such as the Penman or energy balance methods (e.g. Lenters et al., 2005; Shanahan et al., 2007). Direct measurement of lake evaporation using the eddy covariance approach has been applied in relatively few studies. It has been used on several large flow-through lakes (e.g. Blanken et al., 2000; Blanken et al. 2011; Wang et al., 2014), but only a few closed-basin lakes (e.g. Li et al., 2016; Wang et al., 2017). Eddy covariance has relatively few theoretical assumptions and can reveal detailed physical characteristics of lake evaporation at high temporal resolution (i.e. hourly), providing important information needed for the development and optimization of physical models for the broader study and estimation of lake evaporation (e.g. Granger and Hedstrom, 2011; Hu et al., 2017).

Lake evaporation is influenced by atmospheric and lake-surface processes acting at different time scales. At hourly to daily scales, lake evaporation rate is highly correlated to wind speed over the lake and vapor pressure difference between the lake surface and the atmosphere (Blanken et al., 2000; Wang et al., 2017). The mass transfer method uses these two key variables to estimate lake evaporation (Singh and Xu, 1997). At daily to weekly scales, evaporation is influenced by synoptic scale patterns, modulated by the significant thermal lag that results from the high heat capacity of water. For example, cold fronts bringing cold and dry air over a warm lake in fall can significantly enhance evaporation (Blanken et al., 2000; Spence et al., 2013). Seasonal variation in evaporation is mainly forced by changes in net radiation and the air-lake temperature gradient (Lenters et al., 2005). Annual evaporation from temperate closed-basin lakes is particularly sensitive to lake ice phenology. Typically, a longer ice-free period can potentially increase the integrated amount of seasonal evaporation (Rouse et al., 2008). However, observation over large lakes such as Lake Superior and Lake Michigan indicated that temperate lake evaporation is not always positively correlated with ice-free duration (Blanken et al., 2011; Gronewold et al., 2015). For instance, a cold and dry fall season over Lake Superior can significantly enhance the shoulder-season evaporation, cause a large annual total evaporation, and induce a short ice-free season with early ice formation, while a mild winter with a late ice formation may have less cumulative evaporation (Spence et al., 2013). The extent to which these observations apply to much smaller lakes is unclear, and needs to be addressed.

Lake evaporation rates are also influenced by physical properties such as lake geometry (i.e. shape, depth, surface area) and water transparency (e.g. Subin et al., 2012; Deng et al., 2013). Lake depth is an important factor that influences the change in water heat storage and the seasonal phase lag between energy input and evaporation rate. For example, the monthly mean evaporation of a subtropical large shallow lake was closely coupled with seasonal variations in net radiation (Lake Taihu in China, average depth < 2 m, Wang et al., 2014), whereas deep lakes (maximum depth > 10 m) show a 2-to-3-month phase lag between the net radiation and evaporation, regardless of the area of the lake (e.g. Li et al., 2016; Blanken et al., 2000). The transparency or turbidity, which is related to the chemical composition and plankton population distribution within a lake, affects the penetration depth of shortwave radiation, and therefore, the available energy for evaporation (Deng et al., 2013; Wang et al., 2014).

Changes in climate, including air temperature, humidity, wind speed, and available energy, can have an important influence on long-term trends in lake evaporation. The globally average wind speed decreased by 0.7 m s^{-1} from 1950 to 2000, which coincided with an observed decrease in global pan evaporation and calculated crop reference evapotranspiration (McVicar et al., 2012). The global decrease in surface solar radiation (i.e. “global dimming”) between the 1950s and 1980s could also have potentially decreased lake evaporation by reducing the available energy. The more recent “brightening” trend over much of the globe could have acted to enhance evaporation (Wild, 2009). Further, the global mean lake summer surface water temperature was found to increase by 0.34 °C decade $^{-1}$ between 1985 and 2009, correlated with the global brightening and air temperature trends (O’Reilly, et al., 2015). Over the period 1973 to 2003, observed specific humidity over land increased by 0.11 g kg^{-1} per decade, while the relative humidity remained quasi-constant (Willett et al., 2008). Given the observed increases in air temperature and lake surface temperature, this implies that the vapor pressure gradient at the lake surface has also increased. The increase in vapor pressure gradient for the most rapidly warming lakes around the globe was estimated to be 15%–20% from 1985 to 2009 (Friedrich et al., 2018). These trends in key climate variables have likely interacted and influenced lake evaporation, resulting in significant inter-annual variability in lake evaporation and fluctuations in lake water level. Given that multiple trends in atmospheric variables affect the long-term trend of lake evaporation, understanding these trends and projecting future changes requires a physically-based model.

White Bear Lake (WBL) is a typical temperate closed-basin lake in the Mississippi River – Twin Cities watershed, Minnesota, USA. In this watershed, water levels of many lakes have declined significantly during the first decade of this century. A study conducted by the United States Geological Survey (USGS) on 96 lakes in the northeastern Twin Cities Metropolitan Area found that the water levels of 51 flow-through lakes declined an average of 0.2 m from 2002 to 2010, while 45 closed-basin lakes declined by about 0.7 m on average (Jones, et al. 2016). WBL’s water level declined 1.5 m during a 10-year period (2003–2013), and the cause of the decline has been the subject of considerable debate. Proposals to augment the lake water levels have raised serious economic and environmental concerns. A study on WBL’s interaction with groundwater was recently completed by the USGS and Minnesota Department of Natural Resources (MNDNR) (Jones et al., 2013). The annual evaporation was estimated by applying a coefficient of 0.75 to a Class A evaporation pan 18 km away from WBL (Jones et al., 2013). However, estimating annual lake evaporation from a general evaporation pan is a challenging and dubious endeavor (Brustaert, 1982). The single-coefficient method is associated with several potential uncertainties: First, the heat capacity of the evaporation pan is much smaller than that of a large lake; Second, pan evaporation cannot reflect temporal and spatial distributions and vertical profile of lake temperature; Third, although lake evaporation and pan evaporation are both highly correlated with wind speed and vapor pressure gradient above the water surface, these relations differ as the wind-driven mixing influences the evaporation by incorporating the effects of vertical temperature gradient at the lake surface, while a pan is easily well-mixed and the wind-driven mixing maintains temperature homogeneity of the pan (Blanken et al., 2000; Martínez et al., 2006; Roderick et al., 2007).

In this research, we measured and modeled the evaporation at WBL to address the following questions: 1) What is the magnitude of evaporation from a temperate lake and how much does it vary seasonally and inter-annually?; 2) How sensitive is annual evaporation to meteorology and climate and to what extent has evaporation from a temperate closed-basin lake changed over the past 30 years?; 3) How are changes in climate expected to impact evaporation and water level of a temperate closed-basin lake through the 21st Century?; and 4) What are the potential implications for other lakes within the Mississippi River - Twin Cities watershed?

2. Study site

WBL is the second largest lake in terms of surface area (9.7 km^2) in the Twin Cities Metropolitan Area of Minnesota, USA. It is a glacially-formed and trefoil-shaped lake. An island in the west (Manitou Island) and a peninsula in the east divide the lake into three bays: north, west

Table 1
Tabular literature review of studies on evaporation from closed-basin lakes and relevant studies on lake evaporation measured by the eddy covariance method.

	Study	Data/Model used	Lake/Location/Climate/Lake area/Catchment area/ Max. depth/Closed-basin?	Study period	Evaporation rate	Key results/(relation with the four scientific questions of this study)
1	Shanahan et al. (2007)	Penman, the energy budget, and the Priestley–Taylor methods	Lake Bosumtwi/Ghana/Tripical/52 km^2/106 km^2/ 80 m/Yes	1939–2004	1540 mm $year^{-1}$	Lake level to have been caused primarily by changes in precipitation, cloudiness and temperature over the study period./(2, 3)
2	Lenters et al. (2005)	Energy balance	Sparkling Lake/United States/Temperate/ 0.64 km^2/NA/20 m/Yes	1989–1998	3.1 mm day^{-1}	Inter-seasonal changes in evaporation were associated with synoptic weathers. Seasonal variations were driven by temperature and net radiation. Inter-annual changes in summer evaporation rates were associated with changes in net radiation./(1, 2, 3)
3	Sturrock et al. (1992)	Energy budget	Williams Lake/United States/Temperate/0.36 km^2/ 2.27 km^2/9.8 m/Yes	1982–1986	2.2–2.9 mm day^{-1}	Evaporation showed differences in seasonal, annual and inter-annual patterns./(1, 2)
4	Ma et al. (2016)	CRLE model	Nam Co Lake/China/Plateau/1927 ~ 2015 km^2/ 10,610 km^2/over 90 m/Yes	1979–2012	635 mm $year^{-1}$	Significant decrease in lake evaporation was found to be responsible for approximately 4% of the reported rapid water level increase and areal expansion./(2, 3)
5	Zhang et al. (2011)	Penman–Monteith model	Nam Co Lake/China/Plateau/1927 ~ 2015 km^2/ 10,610 km^2/over 90 m/Yes	1976–2009	1184 mm $year^{-1}$	The annual mean evaporation decreased by 40.89 mm $decade^{-1}$ during 1971–2009. Evaporation was always more than precipitation. Climate change, influencing the rainfall and glacial meltwater supply, was an important factor promoting the lake variation./(2, 3, 4)
6	Wang et al. (2017)	EC	A small lake next to Nam Co Lake/China/Plateau/1 km^2/NA/14 m/Yes	2012–2013	812 mm over the ice-free season	Wind speed was significance at half-hourly scale, whereas water vapor and temperature gradients were higher correlated to lake-air turbulent heat at daily and monthly scales. Energy stored during April to June was mainly released during September to November./ (1)
7	Li et al. (2007)	0.69 * pan evaporation	Lake Qinghai/Temperate, semi-arid and cold/ China/4260 km^2/29,660 km^2/25.5 m/Yes	1959–2000	924 ± 10 mm $year^{-1}$	Most dramatic decline in lake level occurred in the warm and dry years, and moderate decline in the cold and dry years, and relatively slight decline in the warm and wet years./(3)
8	Li et al. (2016)	EC	Lake Qinghai/Temperate, semi-arid and cold/ China/4260 km^2/29,660 km^2/25.5 m/Yes	2013–2015	828 mm $year^{-1}$	There was a 2–3 month delay between the maximum net radiation and maximum latent and sensible heat fluxes. Intra-seasonal and seasonal variations in latent and sensible heat flux were strongly affected by different air masses. Changes in wind speed and air temperature were anticipated to change lake evaporation./(1, 2, 3)
9	Vallet-Coulomb et al. (2001)	Penman method and CRLE model	Lake Ziway/Ethiopia/Tropical, sumi-arid to sub-humid/490 km^2/7000 km^2/9 m/No	1969–1990	1730–1870 mm $year^{-1}$	Uncertainties in the results stressed the need for improving the quality of hydrometeorological and chemical time series in semi-arid tropical zones in order to refine hydrological models, and thus allow to accurately predict the impact of future natural and anthropogenic environmental changes in the hydrological systems./(4)
10	Legesse et al. (2004)	Vallet-Coulomb et al. (2001)	Lake Abiyata/Ethiopia/Tropical, sumi-arid to sub-humid/150 km^2/1118 km^2/7–14 m/Yes	1968–1983	1800 mm $year^{-1}$	A comparison of the simulation with and without human consumption indicated that climate variability controlled the inter-annual fluctuations and that the human water use affected the equilibrium of the system by strongly reducing the lake level./(2, 3, 4)
11	van der Kamp et al. (2008)	Multiple studies	16 lakes/Canada/Boreal, semi-arid/0.5–249 km^2/ 116–13,000 km^2/1.8–25 m/Yes	1910–2006	600–900 mm $year^{-1}$	The lake water levels showed overall declines during the twentieth century. Largest year-t o-year decline of the lake water levels occurred in years with little or no runoff to the lakes, low rainfall and strong evaporation./(2)
12	Huybers et al. (2016)	Estimated by pan evaporation	Great Salt Lake/United States/Temperate/ 4300 km^2/55,000 km^2/~10 m/Yes	1957–2000	1000 mm $year^{-1}$	The inter-annual climate variability alone could explain much of the decadal-to-centennial variations in the lake-level record. Evaporation was of secondary importance to precipitation in driving the Great Salt Lake's lake-level changes./(1, 2)
13	Watras et al. (2014)	In-lake evaporation pan and energy balance method in Lenters et al. (2005)	Crystal Lake and Buffalo Lake/United States/ Temperate/ < 0.6 km^2/NA/NA/Yes	1937–2011	370–680 mm $year^{-1}$	The historical oscillation in lake water level has been governed primarily by changes in the net atmospheric flux of water (P-E) and stage-dependent outflow./(2, 3, 4)
14	Wang et al. (2014)	EC	Lake Taihu/China/Subtropical/2400 km^2/NA/NA (mean depth of 1.9 m)/No	2010–2012	1061–1109 mm $year^{-1}$	Unlike boreal deep lakes, the monthly mean sensible and latent heat flux was tightly coupled with seasonal variations in net radiation in this subtropical large shallow lake./(1)

(*continued on next page*)

Table 1 (*continued*)

	Study	Data/Model used	Lake/Location/Climate/Lake area/Catchment area/Max. depth/Closed-basin?	Study period	Evaporation rate	Key results/(relation with the four scientific questions of this study)
15	Blanken et al. (2000)	EC	Great Slave Lake/Canada/Boreal/27,200 km^2/NA/614 m/No	1997–1998	386–485 mm $year^{-1}$	High winds accompanied by cold fronts, resulted in large, episodic evaporation events. The daily total evaporation was best described as a function of the product of the horizontal wind speed and vapor pressure difference between the water surface and atmosphere./(1, 2)
16	Blanken et al. (2011)	EC	Lake Superior/United States/Temperate/82,100 km^2/NA/406 m/No	2008–2010	464–645 mm $year^{-1}$	Evaporation was well described by the ratio of wind speed to vapor pressure. The differences in evaporative water loss between years were largely associated with differences in lake surface conditions (e.g. water temperature, ice cover, and ice duration). Evaporation and ice cover potentially had a negative feedback./(1, 2)
17	Vainu and Terasmaa (2014)	Penman model	Lake Ahnejärv and Lake Martiska/Estonia/Temperate, continental/0.057 and 0.031 km^2/0.45 and 0.14 km^2/9 m and 8.2 m/Yes	1970–2009	648 mm $year^{-1}$	The water-level rise in 1990–2009 was caused by the reduction of groundwater abstraction rates, increased precipitation and decreased evaporation. Climate, catchment vegetation and hydrogeology must all be considered while evaluating the causes of modern water-level changes in lakes./(2)
18	Niedda and Pirastru (2013)	Penman model	Baratz Lake/Italy/Semi-arid Mediterranean/0.6 km^2/12 km^2/16 m/Yes	2008–2011	1188–1287 mm $year^{-1}$	In years with lower than the average rainfall, runoff will be drastically reduced and will not be able to compensate for negative balance between precipitation and lake evaporation./(2)
19	Granger and Hedstrom (2011)	EC/a versatile model	3 Lakes/Canada/Boreal/NA/NA/3–25 m/NA	2005–2009	1.9–3.9 mm day^{-1}	For time periods shorter than daily, the wind speed is the most significant factor governing the evaporation rates, followed by the land-water temperature contrast and the land-water vapor pressure contrast./(1)
20	This study	EC/CLM4-LISSS	White Bear Lake/United States/Temperate/9.7 km^2/19 km^2/25 m/Yes	2014–2016	559–779 mm $year^{-1}$	Daily evaporation at WBL was strongly influenced by synoptic-scale variability. The heat released from the lake was the main energy source for evaporation in the fall. A regional drought and potential intensified groundwater use can have a dramatic impact on water level at a closed-basin lake. Annual evaporation at WBL is expected to increase over this century under the RCP 8.5 scenario, which is largely driven by the extended ice-free periods. A tendency for increased likelihood of lower water levels and greater fluctuations in water level for WBL and other lakes within the region is expected./(1, 2, 3, 4)

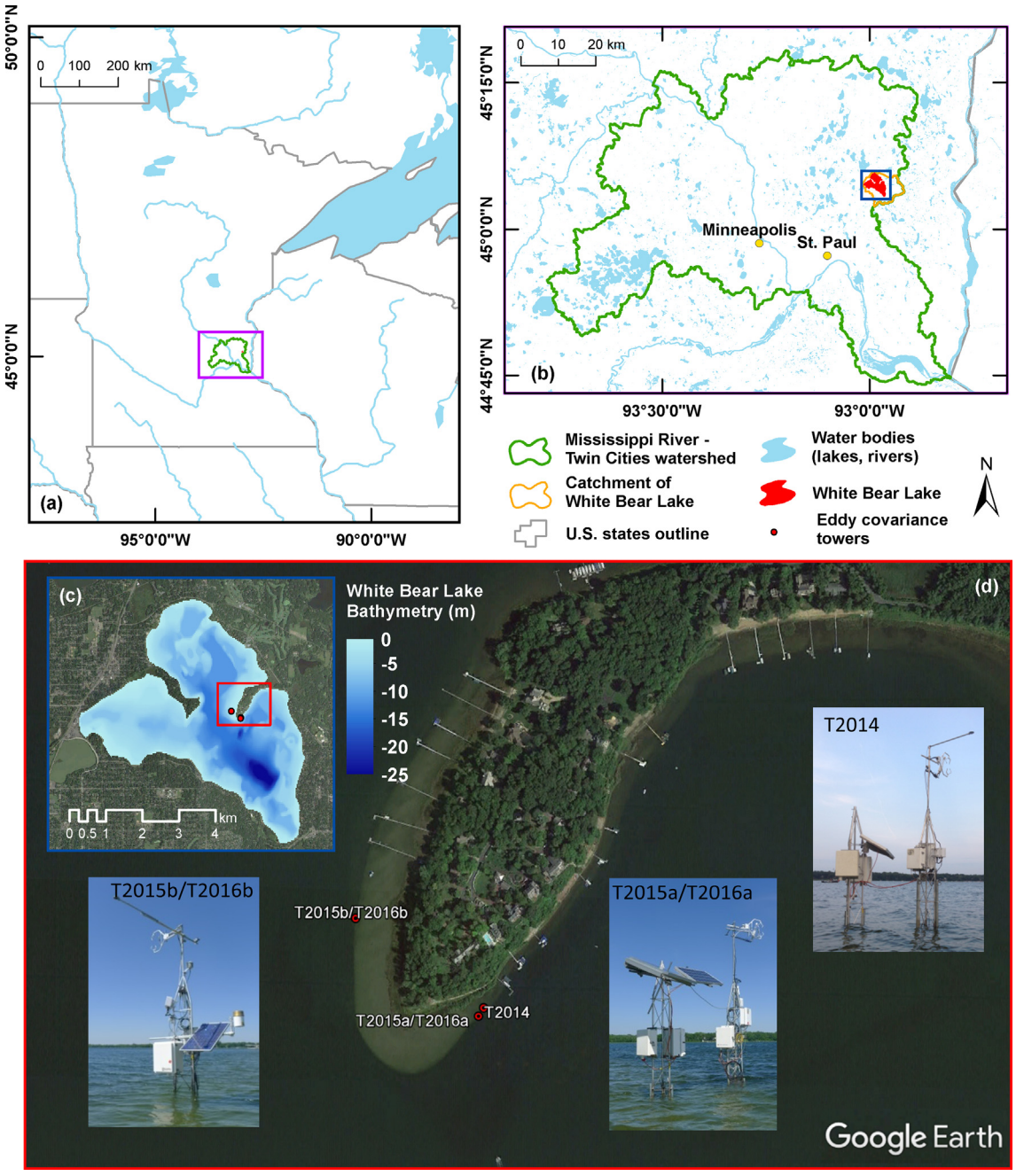

Fig. 1. Regional and local maps of White Bear Lake and location of deployed eddy covariance towers: (a) Minnesota and surrounding area; (b) Mississippi River - Twin Cities watershed and catchment of White Bear Lake; (c) bathymetric map of White Bear Lake; (d) location of eddy covariance towers deployed at White Bear Lake (T2014: Tower location in 2014; T2015a, T2015b: Tower locations in 2015; T2016a, T2016b: Tower locations in 2016). The satellite images in (c) and (d) are snapshots of the historical imagery on August 11, 2015 from Google Earth - © 2017 Google.

and southeast (Fig. 1c). The deepest point is 25 m in the southeast bay; however, the lake depth is generally < 10 m in the north and west bays. There is no natural inlet or outlet around WBL. However, there is a control outlet at a water level of 281.7 m above the sea level, which allows an outflow rate of about 0.12 $m^3 s^{-1}$ for a water level of 282 m (MNDNR, 1998). Three aquifer layers lie below WBL. From top to bottom, these layers include a glacial water-table aquifer in the Quaternary deposits, the St. Peter Sandstone bedrock aquifer, and the Prairie du Chien-Jordan bedrock aquifer. Lake water and groundwater exchange directly in the glacial water-table aquifer, and the water in the glacial water-table aquifer can seep downward to the bedrock aquifers (Jones et al., 2013).

Since WBL is a closed-basin and has a relatively small catchment-to-lake area ratio of 2:1 with a catchment area of 19 km^2, its water level is very sensitive to changes in climate and/or hydrologic conditions. The recent study on WBL's interaction with groundwater suggested that the lake-water discharge to glacial buried and bedrock aquifers was a critical hydrologic sink for WBL (Jones et al., 2013). They found that from 1978 to 2002, precipitation and evaporation could explain the lake level variation, but additional increasing municipal groundwater withdrawals needed to be considered to accurately simulate changes in water level from 2003 to 2011. Their analyses imply that increased groundwater pumping within the region could be an emerging threat to numerous lakes within the region. Furthermore, changes in climate (higher air temperature and humidity, longer ice-free periods, changes in wind speed and net radiation) could significantly enhance

evaporation and thereby amplify declining lake levels during relatively dry or drought periods.

3. Methods

3.1. Observations

3.1.1. Eddy covariance measurements

We installed one eddy covariance (EC) tower in 2014 and two EC towers in 2015 and 2016 (Fig. 1). In 2014, one tower (T2014) was first set up south of the east peninsula (45° 4′38.0″N, 92°58′34.6″W) on July 18. It was removed on November 14 to prevent damage from lake ice formation. The tower was located at the edge of the lake terrace where the water depth was about 1 m. Relatively light-colored sand covers the terrace and dominant aquatic plants such as coontail (*Ceratophyllum demersum*) and Eurasian watermilfoil (*M. spicatum*) (McComas, 2011) that were present in deeper water beyond the terrace.

In 2015, one tower (T2015a) was installed about 14 m away from the 2014 tower location (45° 4′37.6″N, 92°58′34.9″W). The other tower (T2015b) was set up to the west edge of the peninsula terrace (45° 4′42.1″N, 92°58′43.1″W). These two towers were operational from May 8 to October 31. In 2016, we installed EC towers at the same locations as in 2015. The 2016 observations started a week after the ice-out date on March 25 and continued through the frozen period until February 17, 2017.

A three-dimensional sonic anemometer (model CSAT3; Campbell Scientific, Logan, UT) and an open-path CO_2/H_2O gas analyzer (model LI-7500; LI-COR, Lincoln, NE) were installed about 3 m above the water surface at T2014. The sonic anemometer was oriented to the southeast to ensure a relatively broad fetch from the south. The instrument settings on T2015a were nearly identical to T2014, however, a krypton hygrometer (model KH20; Campbell Scientific, Logan, UT) was added for comparison to the LI-7500. T2015b was equipped with a CSAT3 and a KH20, which were installed about 3 m above the water surface. The sonic anemometer was oriented to the northwest in order to observe the fetch from the north. The towers in 2016 used the same instrumentation as in 2015.

All EC signals (wind speed, sonic temperature, and water vapor density) were recorded at 10 Hz. Other variables, including net radiation, water skin temperature, and 1-m water temperature, were measured every 5 s. Flux calculations and corrections followed the methods described in Lee et al. (2004). Fluxes were calculated from the 10 Hz data using block averaging every 30 min and rotated into the natural wind coordinate system using a double rotation (Lee et al., 2004). A correction term for UV absorption by oxygen (Tanner et al., 1993) was applied to water vapor flux estimates of the KH20. The Webb, Pearman and Leuning (WPL) density terms (Webb and Leuning, 1980) were applied to all the turbulent heat flux estimates.

Other ancillary meteorological variables such as net radiation, air pressure, water skin temperature, 1-m water temperature were measured every 5 s. Detailed information of instrumentation for each micrometeorological tower is listed in Table S1.

3.1.2. Filtering and gap-filling

The raw turbulent heat fluxes were filtered using a double difference function following Papale et al. (2006) and Griffis et al. (2016). As another quality control measure to remove outliers, we compared the water vapor concentrations between the LI7500 and the relative humidity sensor (model CS215-L; Campbell Scientific, Logan, UT), and discarded fluxes if the difference was larger than 5%.

Both KH20 sensors exhibited detectable drifts in signal strength related to dirt building up on the lenses and aging detectors. Therefore, we calibrated the KH20 sensors every 10 days by independently comparing their water vapor concentration measurement with two other higher-precision moisture sensors (LI7500 and CS215-L) on each tower.

Finally, since the highest ground elevation of the peninsula is about 15 m above the lake surface, the near-surface wind tends to veer along the shoreline. The EC data were filtered to eliminate any fetch associated with nearby land according to wind rose and flux footprint analyses.

Due to power failure and filtering, about 20% of the half-hourly latent heat flux data were missing over the whole observation period. We applied the Neural Net Fitting in the Neural Network Toolbox in MATLAB 2016a to fit all data from 2014 to 2016, and then used the fitting function to fill gaps. We set 100 hidden nodes and used the Levenberg-Marquardt method (Demuth et al., 2014). The critical input variables for fitting included meteorological variables: air temperature (T_a), vapor pressure (e_a), wind speed (U), and friction velocity (u_*); lake water variables: water skin temperature (T_s), 1-m water temperature (T_w), and lake-surface saturation vapor pressure (e_s); and energy terms: net radiation (R_n) and sensible heat flux (H). Given that the evaporation was influenced by thermal and moisture gradients at the water-air interface, the lake-surface vapor pressure difference ($e_s - e_a$) and temperature difference ($T_s - T_a$) were included. A non-linear term $U(e_s - e_a)$ was also treated as an input variable because evaporation was found to be highly correlated to it in previous studies (Singh and Xu, 1997; Blanken et al., 2000).

3.1.3. Ice phenology

The ice-out date of WBL has been well documented by MNDNR since 1928. However, there are no long-term records for ice-in dates. Two daily 500-m reflectance products (MOD09GA and MYD09GA) from the Moderate Resolution Imaging Spectroradiometer (MODIS) instruments on the Terra and Aqua satellites (Vermote and Wolfe, 2015; Vermote, 2015) were used to determine the ice cover over the lake. The retrieved ice-period data were used to test the ability of CLM4-LISSS to simulate the ice cover over WBL (described further below). The averaged time series of the two products were used to calculate the daily normalized difference snow index (NDSI) following Irish (2000):

$$NDSI = \frac{band\ 2 - band\ 5}{band\ 2 + band\ 5} \quad (1)$$

where bands 2 and 5 are reflectances in the near infrared (841–876 nm) and shortwave infrared (1230–1250 nm) ranges, respectively. The ice phenology over WBL was characterized by the NDSI difference between water and land. First, the NDSI of each grid cell within an area of 5 km × 4.5 km around WBL was calculated. Then the grid cells were classified as water or land according to the MODIS 500-m land cover type product MCD12Q1 (Friedl et al., 2010). On clear days, the ensemble average of NDSI over the ice-free water was generally smaller than that over land, while the frozen-lake NDSI was larger than the land NDSI. On cloudy days, the differences of NDSIs between land and water were close to zero. Therefore, the NDSI difference between water and land is generally negative when the lake is open and positive when the lake is frozen. Ice-in and ice-out dates were determined by the inflection points in the yearly cumulative series of the daily NDSI difference. The ice-in dates fall near the yearly minimum of the accumulation, while the maximum indicates the ice-out events. The major sources of uncertainty are cloud cover, snow events, and the enduring time of freezing and thawing. Clouds, snow on land, and partial ice-cover over the lake can minimize the NDSI difference, causing the ice-in/out dates to differ from the actual minima/maxima points. Because the ice-in process is generally longer than for ice-out, there is greater potential for a bias in estimating the ice-in date.

3.2. Modeling

3.2.1. Model description

The Community Land Model version 4 – Lake, Ice, Snow and Sediment Simulator (CLM4-LISSS) is the offline lake model in CLM 4.5 (Subin et al., 2012; Oleson et al., 2013). Although this model is a one-dimensional lake model that only considers mixing in the vertical

direction, it has shown reasonable performance in simulating lake temperature and surface energy fluxes for several different sized lakes around the world (e.g. Subin et al., 2012; Deng et al., 2013; Stepanenko et al., 2014; Hu et al., 2017). The version of CLM4-LISSS we used here was based on Deng et al. (2013) and Hu et al. (2017). The model was tuned and validated to reproduce the observed WBL evaporation from 2014 through 2016 in order to perform retrospective analyses of evaporation extending from 2016 back to 1979, and to predict future evaporation from 2017 to 2100.

3.2.2. Forcing data and model spin-up

CLM4-LISSS is forced by seven variables including air temperature, air pressure, air humidity, precipitation, wind speed, down-welling shortwave radiation and down-welling longwave radiation. In the model validation test, CLM4-LISSS was primarily forced by climate data obtained from the EC systems and nearby local weather stations. Air temperature, pressure, humidity, and wind speed were obtained from 2014 to 2016 using the EC measurement systems (Table S2). The gaps in these variables were filled using simple linear regression with data from a nearby Citizen Weather Observer Program (CWOP) weather station EW2811 (45° 7′ 58″ N, 93° 0′ 39″ W), which is located about 6.8 km to the northwest of T2014. The observations of air temperature, pressure, humidity and net radiation in 2015 and 2016 showed that these values were highly consistent between the towers, so the averages of these variables from both towers were used to drive the model. The wind speed was chosen from representative fetches of the towers determined by the wind roses and flux footprints. Precipitation and down-welling shortwave radiation were measured in 2015 and 2016 but not in 2014, and the down-welling longwave radiation was not measured during the three years. Periods without observations were gap-filled using the reanalysis product of the hourly 0.125×0.125°North American Land Data Assimilation System (NLDAS) Primary Forcing Data (NLDAS_FORA0125_H) (Xia et al., 2012).

Due to the coarse resolution of the NLDAS data, the grid cell containing WBL mainly reflected features over land rather than water. The diurnal features of air temperature and specific humidity in the NLDAS data were not consistent with our observations from 2014 to 2016. Overall, the daily peak of the air temperature in the NLDAS data was roughly 3-h earlier than that over WBL. The amplitudes of the diurnal variation in air temperature were larger than the observations. The daily averages of specific humidity in the NLDAS data were generally smaller than the observations. Consequently, we used the Neural Net Fitting in the Neural Network Toolbox in MATLAB 2016a with 10 hidden nodes and the Levenberg-Marquardt method (Demuth et al., 2014) to fit the observations with the NLDAS data and obtain the fitting function. The fitting function was then used to correct the air temperature and specific humidity in the entire dataset. The correction did not introduce or change long-term trends of the original data. Furthermore, Piecewise Cubic Hermitian Polynomial interpolation (Fritscht and Carlson, 1980) was applied on the NLDAS data to obtain half-hourly values.

The water temperature profile in the upper lake levels can be obtained with a spin-up time of about 1 month. However, we found that the temperature in the deepest part of the lake required 3–5 years to reach thermal equilibrium. Therefore, NLDAS data from 2004 to 2013 were applied for the model spin-up in the validation simulations.

3.2.3. Model tuning

In the model validation, we optimized the model by tuning its parameters and assessing if CLM4-LISSS produces similar variability in evaporation due to climate when compared to the observations. CLM4-LISSS simulates the sensible heat flux and the latent heat flux using the aerodynamic method (Subin et al., 2012). The sensible heat flux is computed from the thermal resistance and the temperature difference between surface air and the lake surface. Similarly, the latent heat flux is determined by the moisture resistance and the vapor pressure difference at the lake surface. The aerodynamic resistance terms are computed from Monin–Obukhov similarity theory, with prescribed roughness lengths of momentum, heat and moisture.

Since the atmospheric temperature and moisture are driven by the forcing data, the modeled lake skin temperature will critically determine the temperature and the vapor pressure differences at the lake surface. The lake skin temperature is iteratively solved to close the energy balance within a conceptual lake surface layer. The model assumes that this layer absorbs the penetrated shortwave radiation with an absorption fraction (β), which is related to the light extinction coefficient (η) of the lake and the thickness of this surface layer (z_a) by Beer's law (Deng et al., 2013):

$$\beta = 1 - e^{-z_a \eta} \tag{2}$$

The extinction coefficient can be estimated as $1.7/S_d$, where S_d is Secchi Disk transparency (Boyd, 2015). The Minnesota Pollution Control Agency (MPCA) occasionally recorded the transparency at WBL during the ice-free seasons from 1974 to 2015, using an all-white, 20-cm-diameter Secchi Disk. The observed transparency varied between 2 and 10 m, and the annual median value ranged between 1.5 and 4.5 m. No significant annual trend was found within the whole observation period. The 40-year average of the annual median is about 3 m. In our simulations, the extinction coefficient was thus set as a constant of $0.57\ \mathrm{m}^{-1}$.

A surface layer thickness of 0.6 m is generally set in CLM4-LISSS, and this value has been validated for various lakes around the world (e.g. Subin et al., 2012). Deng et al. (2013) reported that for a shallow (about 2 m) and turbid lake ($\eta = 5\ \mathrm{m}^{-1}$), the conceptual thickness can be as small as 0.2 m. Because WBL is generally deeper and relatively clear, we assumed that the general setting of 0.6 m was reasonable for our simulations.

While β is set fixed, the lake skin temperature is sensitive to the thermal diffusivity of the water. This diffusivity is a critical parameter to tune, because it represents both vertical and horizontal mixing. In the model, the diffusivity is the sum of molecular, wind-driven eddy and enhanced eddy diffusivities. Here the dominant term is wind-driven eddy diffusivity, which is large at the surface and decreases exponentially with depth (Henderson-Sellers, 1985). The enhanced eddy diffusivity is a parameterization of the unresolved 3D mixing (Fang and Stefan, 1996).

Sensitivity analyses revealed that the lake skin temperature was most sensitive to the wind-driven eddy diffusivity, and that the amplitude of the simulated diurnal variation of lake skin temperature was too small in the original scheme. Simulations were substantially improved after reducing the wind-driven eddy diffusivity to 0.5% of its original scheme. This yielded a surface wind-driven eddy diffusivity that typically varied between 0.1×10^{-5} and $1.8 \times 10^{-5}\ \mathrm{m^2\,s^{-1}}$. Deng et al. (2013) reported a similar feature and they scaled the original scheme by 2% (i.e. eddy diffusivity ranged from 0.1×10^{-5} to $4 \times 10^{-5}\ \mathrm{m^2\,s^{-1}}$) for a large shallow lake. They found that the large wind-driven eddy diffusivity erodes the stratification and causes smaller diurnal variation in the lake skin temperature. Furthermore, the lake skin temperature in the fall is very sensitive to the diffusivity in the deeper part of the lake. The analyses revealed that the original enhanced eddy diffusivity was appropriate for WBL, although Subin et al. (2012) proposed that the enhanced eddy diffusivity should scale by a factor of 10 for a deep lake.

The tunings of diffusivity implied that although the deepest point of WBL is 25 m, the deep lake setting cannot be entirely applied to WBL. WBL is a V-shaped glacial lake, and its uneven topology causes a range of mixing properties. The wind-driven mixing is not efficient in shallow regions of WBL, while the deep parts of the lake store significant heat and impact the seasonal and annual temperature variability. Further, given the relatively small fetch of WBL, the surface wind and internal boundary layer might not be fully equilibrated above the lake surface, and therefore, might not effectively drive the eddy mixing within the

lake surface layer.

After tuning the diffusivity, the aerodynamic roughness lengths were then tuned to better reproduce the turbulent heat fluxes. Our tuning yielded optimized values for the roughness lengths of momentum (z_{0m}), heat (z_{0h}) and moisture (z_{0q}) in the dynamic ranges of 10^{-5}–10^{-4} m, 10^{-7}–10^{-8} m, and 10^{-7}–10^{-8} m, respectively. Furthermore, $\ln(z_{0m}/z_{0h})$ and $\ln(z_{0m}/z_{0q})$ were kept constant as 7.36 and 7.48, respectively.

3.2.4. Retrospective modeling

In the retrospective simulations, the optimized CLM4-LISSS was driven by the NLDAS data from 1979 to 2016. The air temperature and specific humidity in the NLDAS was corrected by the method described in the Section 3.2.2. The data from 1980 were cycled over a ten-year period to initialize the model.

3.2.5. Projected modeling

To investigate future changes in lake evaporation and water level in response to anticipated climate change, we used the tuned CLM4-LISSS to predict the WBL evaporation under the Representative Concentration Pathways RCP8.5 ("Business as usual") greenhouse gas emission scenario (Riahi et al., 2011) from 2017 to 2100. The forcing data were 3-hourly outputs from the GFDL-ESM2G climate model (Dunne et al., 2012) in the fifth phase of the Coupled Model Inter-comparison Project (CMIP5). These simulations were performed for years 2006 to 2100. Data from 2006 to 2016 were used for model initialization and spin-up.

4. Results

4.1. Observed evaporation

4.1.1. Climatology

Monthly temperature and precipitation data for the Twin Cities Metro Area from 2014 to 2016 are shown in Fig. 2 and compared with the climate normal for the period 1981–2010 (National Weather Service Forecast Office's Now Data: NOAA Online Weather Data, http://w2.weather.gov/climate/xmacis.php?wfo=mpx). The mean annual air temperature in 2014 was 1.6 °C cooler than the climate normal (7.8 °C) and 2015 was 1.2 °C warmer than the climate normal. Each month in 2016 was warmer than normal except December. The mean annual temperature in 2016 was 2 °C warmer than normal. The annual precipitation totals from 2014 to 2016 were 899 mm, 918 mm and 1024 mm, respectively. Each year had greater than normal (777 mm) precipitation. In 2014, the precipitation was mainly concentrated in late spring and early summer, while both 2015 and 2016 experienced higher than normal precipitation in summer and fall.

Due to the warmer spring and fall, 2015 and 2016 both had significantly earlier ice-out dates and later ice-in dates than in 2014. According to the MNDNR ice phenology data, there was no significant trend in the ice-out dates of WBL from 1979 to 2016 (slope = -0.156 day year^{-1}, p = 0.319) (Fig. 3). The ice-out dates retrieved from MODIS were in good agreement with the MNDNR observations (MODIS vs. MNDNR: slope = 1.097, R^2 = 0.98, p < 0.01) in the period 2000–2016. Both ice-in dates and ice-free days from MODIS indicate no statistically significant trends from 2000 to 2016 (slope = -0.561 day year^{-1}, p = 0.189 for ice-in dates; and slope = -0.390 day year^{-1}, p = 0.676 for ice-free days).

4.1.2. Energy budgets

The mean monthly energy balance partitioning is shown in Fig. 4. The net radiation peaked at 160 W m^{-2} in June and July and dropped below 20 W m^{-2} in November. Except for a short period after ice-out (e.g. March 2016), the sensible heat flux was positive (upward). The sensible heat flux reached its annual maximum (21–25 W m^{-2}) in October (in 2015 and 2016) or November (in 2014). The latent heat flux was always larger than the sensible heat flux in the ice-free season. It gradually increased from spring to mid-summer and reached a maximum of 110–129 W m^{-2} between July and August, and slowly decreased from 80 to 90 W m^{-2} in the summer to 30–40 W m^{-2} in the fall.

We were not able to measure lake water temperature profiles to adequately calculate changes in the WBL heat storage. Instead, we calculated the energy residual by subtracting the turbulent heat fluxes from the net radiation (i.e. $\Delta S = Rn - H - LE$) and used it to estimate the heat storage change. A positive energy residual indicates an increase in lake heat storage while a negative residual indicates that energy was released and transformed into turbulent heat fluxes. Here we assumed that our EC measurements underestimated the total turbulent heat flux by 20% based on energy balance closure analyses

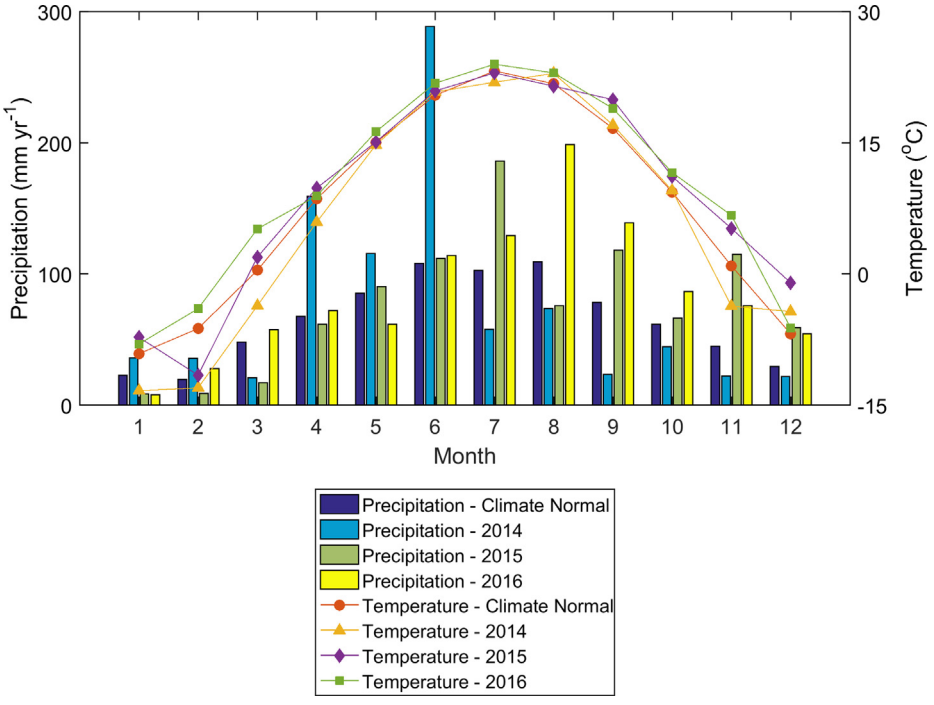

Fig. 2. Climate Normal (1981–2010) for monthly precipitation and air temperature in Twin Cities Metro Area, MN. Observed monthly air temperature and precipitation for years 2014–2016 are also shown (National Weather Service Forecast Office's Now Data: NOAA Online Weather Data, http://w2.weather.gov/climate/xmacis.php?wfo=mpx).

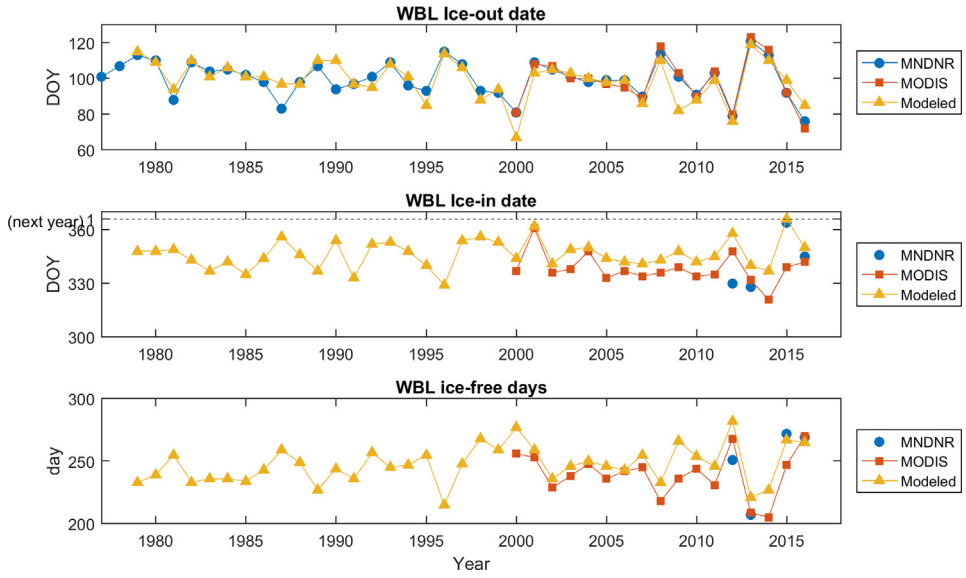

Fig. 3. Ice-in, ice-out dates and length of ice-free period at White Bear Lake based on Minnesota Department of Natural Resources records, MODIS estimates, and retrospective modeling.

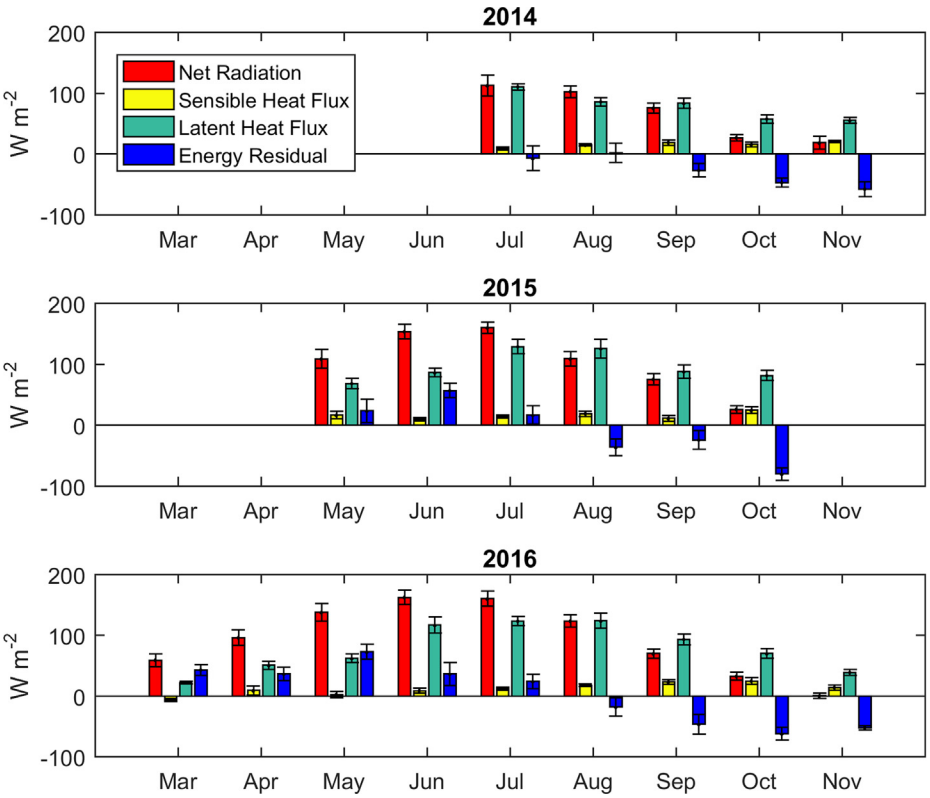

Fig. 4. Measured monthly energy balance components at White Bear Lake for 2014–2016.

(Wilson et al., 2002; Nordbo et al., 2011).

From spring to mid-summer, the positive residuals indicated that the net radiation warmed the lake and increased the heat storage. From late summer to fall, while the net radiation gradually reduced to zero, the increased negative residuals indicated that the heat released from the lake became the energy source driving the turbulent fluxes.

4.1.3. Daily evaporation patterns

The pattern of the 24-h total daily evaporation (i.e. the daily evaporation rate) is shown in Fig. 5. Daily evaporation rates were impacted by synoptic-scale variabilities in air temperature, humidity, and wind speed. During summer, the distinct spikes in evaporation were induced by the passing of cold fronts (Blanken et al., 2000; Spence et al., 2013). The peaks of evaporation with daily wind speeds $> 2\,m\,s^{-1}$, positive temperature gradients, and vapor pressure gradients were typically triggered by the passage of cold fronts. During the observation period, such events were identified 7 times in 2014, 14 times in 2015, and 21 times in 2016. These events occurred in October most frequently, 3 times in 2014, 4 times in 2015 and 5 times in 2016. A pronounced two-week cycle of evaporation in the fall coincided with synoptic scale systems as identified by wavelet time-series analyses in 2015 and 2016 (Figs. S4–S6).

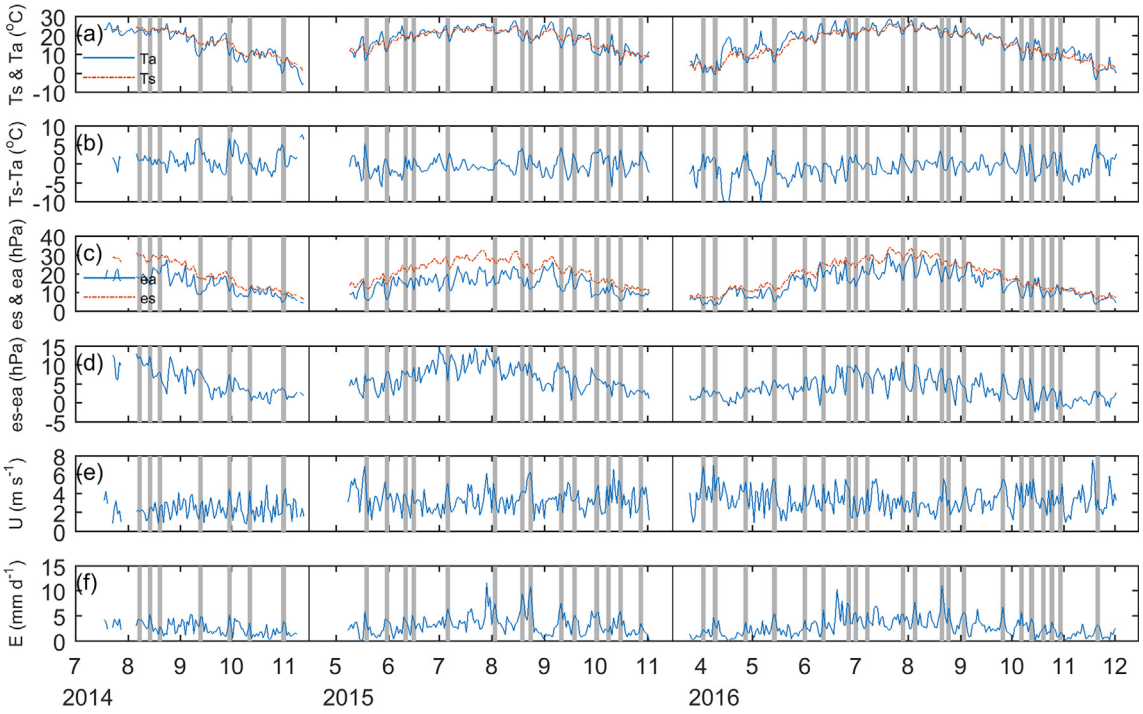

Fig. 5. Comparison of daily environmental variables during the 2014–2016 observation period: (a) air temperature (T_a) and lake skin temperature (T_s); (b) lake-surface temperature difference ($T_s - T_a$); (c) atmospheric vapor pressure (e_a) and lake-surface saturated vapor pressure (e_s); (d) lake-surface vapor pressure difference ($e_s - e_a$); (e) Wind speed at 3 m (U); and (f) evaporation (E). The peaks of evaporation with daily wind speeds $> 2\,m\,s^{-1}$, positive temperature gradients, and positive vapor pressure gradients are indicated by gray shadows.

4.1.4. Annual evaporation

To quantify the annual evaporation from 2014 to 2016, the primary challenge is to estimate the evaporation that occurred outside of the observation period. Four approaches were used to help constrain the annual evaporation from 2014 to 2016 (Table 2). The first estimate simply multiplied the observed length of the ice-free period by the measured daily mean evaporation rate. The daily mean of the observation period was calculated from the gap-filled half-hourly data, and the ice-in and ice-out dates were retrieved from the MNDNR and the MODIS data. The second approach applied monthly weighting factors to extrapolate the evaporation to the spring and fall periods when observations were not available. Here, we averaged three years of measurements from March to November and calculated the monthly factors weighted by the total evaporation in August through October, when our observations were nearly continuous among the three years. The other two methods applied CLM4-LISSS to extrapolate the evaporation beyond the observation period. The third estimate used the optimized CLM4-LISSS model, which was forced with local observations. The fourth method was derived from the retrospective modeling approach with CLM4-LISSS forced only with the reanalysis data product.

The first method resulted in evaporation estimates of 543 mm, 915 mm, and 778 mm for 2014 to 2016, respectively. This simple annual estimate represents an upper bound on evaporation and contains two main uncertainties: the observation errors and the errors associated with the extrapolation of the observation data to the early and late ice-free periods. For example, in 2015, our observations captured much of the summer season, but missed the shoulder seasons, which likely had less evaporation due to lower available energy. The second approach estimated evaporation in the three years to be 535 mm 763 mm and 748 mm, respectively. The annual evaporation estimated from method three was 567 mm, 709 mm and 773 mm for the three years. Finally,

Table 2
Annual evaporation estimates for White Bear Lake from 2014 to 2016.

Year & Observation Period (days[×])	Sources of Evaporation and ice phenology data	Ice-out date	Ice-in date	Ice-free days	Daily E (mm)	Annual E (mm)
2014	EC, MNDNR	Apr 23	*Nov 17	209	2.60	543
Jul 18	Weighted EC, MNDNR	Apr 23	*Nov 17	209	2.56	535
to Nov 14	Validation modeling	Apr 22	Nov 28	221	2.57	567
(102)	Retrospective modeling	Apr 20	Dec 3	228	2.59	590
2015	EC, MNDNR	Apr 2	Dec 30	273	3.35	915
May 8	Weighted EC, MNDNR	Apr 2	Dec 30	273	2.79	763
to Oct 31	Validation modeling	Apr 3	Dec 16	258	2.75	709
(177)	Retrospective modeling	Apr 9	(2016) Jan 1	268	2.73	731
2016	EC, MNDNR	Mar 16	Dec 10	270	2.88	778
Mar 25	Weighted EC, MNDNR	Mar 16	Dec 10	270	2.77	748
to Nov 30	Validation modeling	Mar 13	Dec 15	278	2.78	773
(251)	Retrospective modeling	Mar 25	Dec 15	266	2.87	764

[×] The integrated days does not include the missing days within observation period.
* No record from MNDNR, filled by the MODIS data.

method four resulted in annual estimates of 590 mm, 731 mm and 764 mm. Overall, these estimates were relatively consistent excluding method one for 2015, which resulted in a large overestimate. The major difference between the modeled and weighted estimates was caused by the ice phenology. The model overestimated the length of the ice-free days in 2014, and underestimated the length in 2015.

After averaging the four estimates for each year, and applying the standard variance as the error of uncertainty, we estimated the annual evaporation in the three years at WBL to be 559 ± 22 mm, 779 ± 81 mm, and 766 ± 11 mm, respectively. The annual evaporation in 2014 was least among the three years because of a relatively short ice-free period combined with lower daily evaporation rates.

These estimates did not account for sublimation occurring during the ice cover period. In winter 2016–2017, we made EC measurements over the ice from the end of January to early February, which showed that the monthly latent heat flux was about 5 W m^{-2}. This is equivalent to about 20 mm of evaporation when assuming a 4-month ice-cover period. Sublimation, therefore, represented < 5% of the annual evaporation budget.

4.2. Retrospective evaporation

4.2.1. Model validation

The tuned model, forced by local observations, reproduced the latent heat flux reasonably well from half-hourly to monthly time scales (Fig. 6). At the half-hourly scale, the model explained 74% of the variance, and the Root Mean Square Error (RMSE) was 35 W m^{-2}. At the daily scale, the model performed slightly better with R^2 = 81% and RMSE = 23 W m^{-2}. The errors are mainly contributed by four summer days with high evaporation on Aug 19, 2015, Aug 24, 2015, Jun 20, 2016 and Aug 21, 2016, underestimating the daily mean latent heat flux by over 80 W m^{-2}. Overall, the modeled monthly latent heat flux showed good agreement with observations in spring and fall. However, modeled evaporation was biased low in most summers and it was underestimated in summer 2016 by about 10%.

4.2.2. Retrospective results

The annual water budget terms were calculated based on the retrospective model outputs and the WBL precipitation and water level recorded by MNDNR over the period 1979 to 2016 (Fig. 7). The mean annual precipitation was 868 mm with no significant trends during this period. The mean annual total evaporation was 688 mm, and it increased 3.8 mm $year^{-1}$ ($p < 0.01$). The trend in the annual evaporation was mainly attributed to the increased daily mean evaporation (slope = 0.01 mm day^{-1} $year^{-1}$, $p < 0.01$). During this period, the increase of daily mean evaporation was driven by both increased wind speed (slope = 0.011 m s^{-1} $year^{-1}$, $p < 0.01$) and the lake-surface vapor pressure difference (slope = 0.013 hPa $year^{-1}$, p = 0.095). The increase of the vapor pressure difference was mainly driven by the increased air temperature during the ice-free period (slope = 0.020 °C $year^{-1}$, p = 0.075), while no significant trends were shown in the forcing specific humidity (slope = 0.0032 g kg^{-1} $year^{-1}$, p = 0.51) and the modeled lake surface temperature (slope = 0.0021 K $year^{-1}$, p = 0.81).

The modeling results also show that the length of ice-free period was extended (slope = 0.40 day $year^{-1}$, p = 0.067) over the period 1979 to 2016, with earlier ice-out dates (slope = − 0.294 day $year^{-1}$, p = 0.0734) and insignificant earlier ice-in dates (slope = − 0.156 day $year^{-1}$, p = 0.319) (Fig. 3). The extension of the ice-free period was mainly driven by the increased whole-year air temperature (slope = 0.038 °C $year^{-1}$, p = 0.015). The modeled ice-out dates are largely matched with the MNDNR record (MODIS vs. MNDNR: slope = 0.883, R^2 = 0.68, $p < 0.01$). The trend of the measured ice-out dates in the MNDNR record, while it has the same sign as the modeled trend, is smaller and of lesser significance (slope = −1.29 day $year^{-1}$, p = 0.124).

The difference between observed precipitation and modeled evaporation ($P - E$) showed a similar pattern to the yearly WBL water level change. Linear regression showed that 77% of the lake water level change could be explained by $P - E$ (slope = 1.36, intercept = −247 mm $year^{-1}$, $p < 0.01$). The groundwater inflow to the lake was estimated from the budget residual by assuming a simplified water balance $G(inflow) = \Delta L - P + E$, where ΔL is the change in water

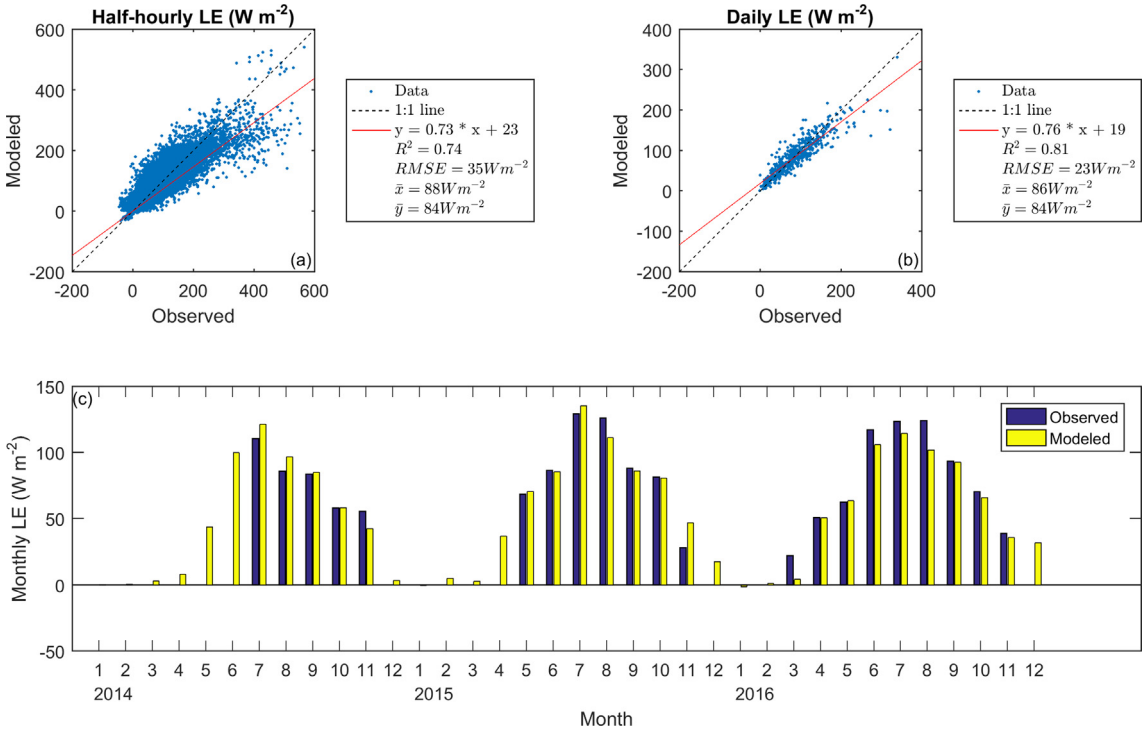

Fig. 6. Comparison of latent heat flux between model simulations and observations at different time scales: (a) half-hourly; (b) daily; and (c) monthly.

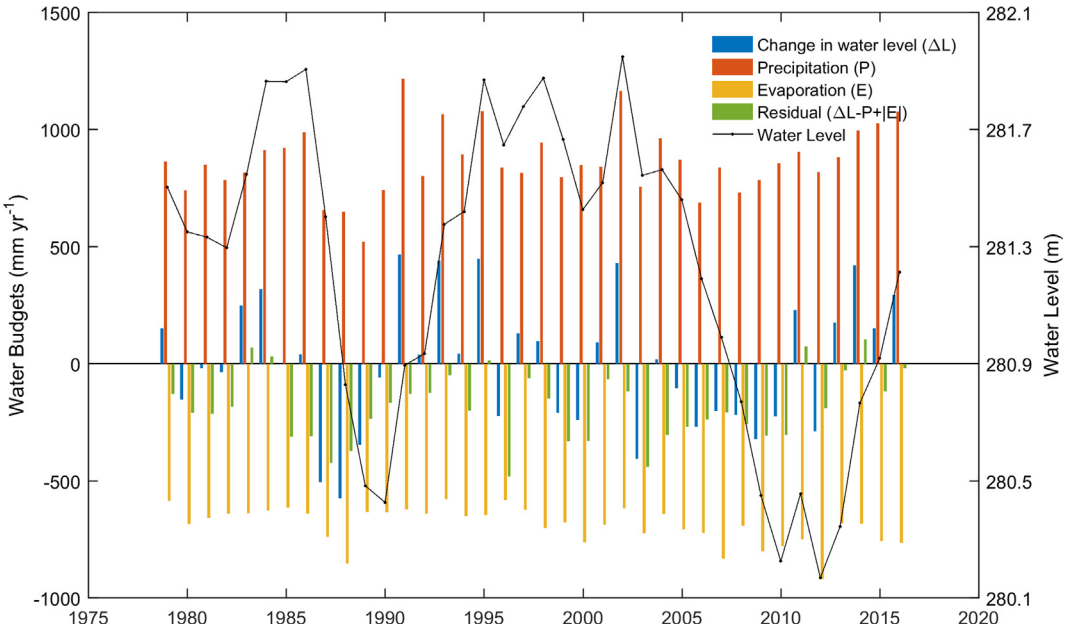

Fig. 7. Water budgets derived from observations and model outputs. Precipitation is from observation and evaporation is from the retrospective modeling. The negative evaporation presented here indicates a positive water vapor flux from the lake to the atmosphere. Water level is the average of observations from November and December in each year. The change in water level is the water level difference between the labeled year and the year before. A positive residual indicates a flux of groundwater to the lake (positive *G*(*inflow*)), and a negative residual indicates lake water seepage into the groundwater.

level, and a positive *G*(*inflow*) indicates a flux of groundwater to the lake. The residual analyses provided a rough estimate of the exchange between lake water and groundwater. The mean annual residual was $-211\,\mathrm{mm\,year^{-1}}$ for the period 1981 to 1990, which is in close agreement ($-283\,\mathrm{mm\,year^{-1}}$, $r = 0.69$, $p = 0.016$) with estimates from a hydrologic model that had comprehensive runoff and groundwater components but a rough evaporation component (MNDNR, 1998). The mean annual residual was $-183\,\mathrm{mm\,year^{-1}}$ for the period 1979 to 2016. This indicates that lake water was generally seeping into the aquifer.

4.3. Projected evaporation

The future WBL evaporation under the RCP8.5 greenhouse gas emission scenario is shown in Fig. 8. Under this scenario, the annual evaporation is expected to increase, mainly due to the longer ice-free period. In the forcing data, the air temperature increased by $0.049\,^{\circ}\mathrm{C\,year^{-1}}$ ($p < 0.01$) and the specific humidity increased by $0.021\,(\mathrm{g\,kg^{-1}})\,\mathrm{year^{-1}}$ ($p < 0.01$). These trends are consistent with the ongoing and expected intensification of the hydrological cycle under a warming climate (Santer et al., 2007; Trenberth and Asrar, 2014). The modeled increase in the ice-free period was $0.50\,\mathrm{d\,year^{-1}}$ ($p < 0.01$), with no significant trend in the daily mean evaporation rate. The combined effect will result in an increase in annual total evaporation of $1.4\,\mathrm{mm\,year^{-1}}$over this century. By the end of this century, the ice-cover days are expected to decrease by more than a month, and the annual evaporation will increase by about 15% ($100\,\mathrm{mm\,year^{-1}}$), equivalent to $9.8 \times 10^5\,\mathrm{m^3}$ of water.

The lack of a significant trend in daily mean evaporation may seem counterintuitive, but most climate models assume, supported to this point by evidence, that as global temperature increases, mean relative humidity is conserved (Allen and Ingram, 2002). Thus, expected increases in mean lake surface vapor pressure (driven by the increases in lake surface temperature with slope $= 0.018\,\mathrm{K\,year^{-1}}$ and $p < 0.01$) will be accompanied by increases in mean atmospheric vapor pressure, so that the lake-surface vapor pressure gradient is projected to increase by only $0.0043\,\mathrm{hPa\,year^{-1}}$ ($p = 0.17$). Further, wind speed is expected to decrease by $0.0019\,\mathrm{m\,s^{-1}\,year^{-1}}$ ($p < 0.01$), and the average net radiation during the ice-free period is forecast to decrease by $0.039\,\mathrm{W\,m^{-2}\,year^{-1}}$ ($p = 0.099$).

5. Discussion

5.1. Observed evaporation

5.1.1. Evaporation rates and patterns

During the observation period, the estimated average daily evaporation rate during the ice-free season ranged from 2.6 to $3.4\,\mathrm{mm\,day^{-1}}$ from WBL (Table 2), similar to values reported for small temperate closed-basin lakes such as Sparkling Lake and Williams Lake listed in Table 1. The WBL annual evaporation rate ranged from 559 to $779\,\mathrm{mm\,year^{-1}}$, similar to Lake Ahnejärv and Lake Martiska in Europe, with average annual evaporation rates of $648\,\mathrm{mm\,year^{-1}}$ from 1970 to 2009 (Vainu and Terasmaa, 2014).

The patterns of evaporation at WBL showed many features common to other closed-basin lakes (Table 1). Similar dynamics between heat storage changes and turbulent heat fluxes have been reported previously for a broad range of lake types (e.g. Blanken et al., 2000; Lenters et al., 2005; Li et al., 2007; Gianniou and Antonopoulos, 2007; Spence et al., 2013; Wang et al., 2014; Wang et al., 2017). A one-month phase lag between latent heat flux and net radiation was also observed over Sparkling Lake, a small temperate closed-basin in the Upper Midwest US (Lenters et al., 2005), while a lag of two to three months has been observed over large deep lakes such as Lake Superior in the US (Blanken et al., 2000) and Lake Qinghai in China (Li et al., 2007). The energy stored in WBL from May to July, and released from September to November, was similar to that observed from a small plateau closed-basin lake in China (Wang et al., 2017).

However, the influence of the length of the ice-free period on annual and inter-annual variation in evaporation from temperate closed-basin lakes was not well characterized in the studies summarized in Table 1. Our study found that the ice phenology is an important factor for estimating the annual total evaporation and it is an important causal factor of the inter-annual differences in annual evaporation.

The annual total evaporation (E_{annual}) is the product of daily mean evaporation rate in the ice-free period (E_{day}) and the length of ice-free

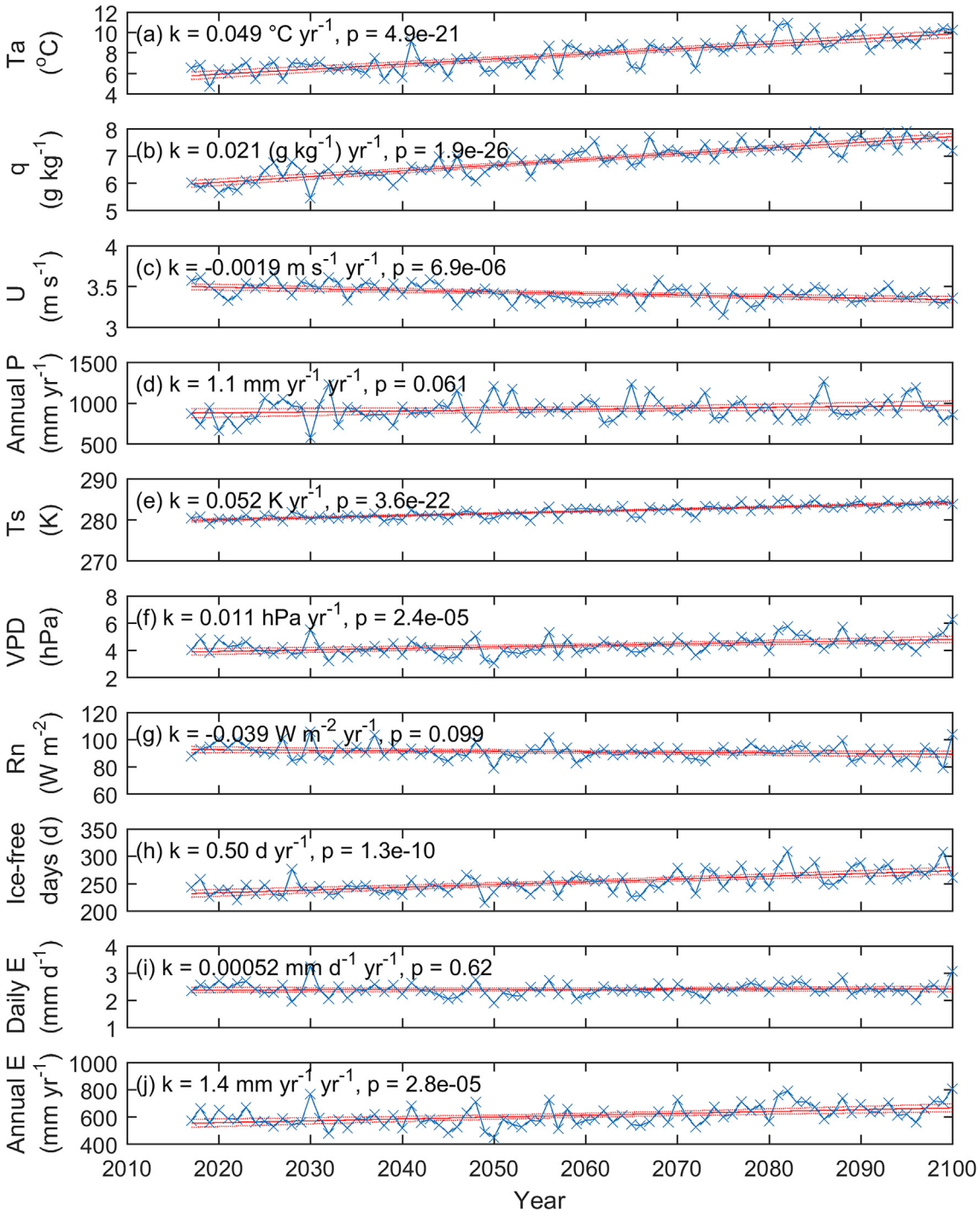
Ta (°C)
(a) k = 0.049 °C yr-1, p = 4.9e-21
q (g kg-1)
(b) k = 0.021 (g kg-1) yr-1, p = 1.9e-26
U (m s-1)
(c) k = -0.0019 m s-1 yr-1, p = 6.9e-06
Annual P (mm yr-1)
(d) k = 1.1 mm yr-1 yr-1, p = 0.061
Ts (K)
(e) k = 0.052 K yr-1, p = 3.6e-22
VPD (hPa)
(f) k = 0.011 hPa yr-1, p = 2.4e-05
Rn (W m-2)
(g) k = -0.039 W m-2 yr-1, p = 0.099
Ice-free days (d)
(h) k = 0.50 d yr-1, p = 1.3e-10
Daily E (mm d-1)
(i) k = 0.00052 mm d-1 yr-1, p = 0.62
Annual E (mm yr-1)
(j) k = 1.4 mm yr-1 yr-1, p = 2.8e-05
2010 2020 2030 2040 2050 2060 2070 2080 2090 2100
Year

Fig. 8. Forcing data and modeling results based on the RCP 8.5 scenario: (a) annual mean air temperature; (b) annual mean air specific humidity; (c) annual mean surface wind speed; (d) annual cumulative precipitation; (e) modeled annual mean lake water skin temperature; (f) modeled annual mean lake-surface vapor pressure difference; (g) modeled annual mean net radiation in ice-free seasons; (h) length of ice-free period; (i) daily mean evaporation in ice-free seasons; and (j) annual cumulative evaporation in ice-free seasons. Blue solid lines and crosses indicate yearly data points, while the red solid lines show the linear regression trend; and the red dotted lines indicate the 95% confidence bounds of the trend lines. (For interpretation of the references to colour in this figure legend, the reader is referred to the web version of this article.)

days ($L_{ice\text{-}free}$). Here, we define p, q, and r as the increase ratios of the daily mean evaporation rate, the length of ice-free period, and the total annual evaporation, respectively.

$$E_{annual} = E_{day} L_{ice-free} \tag{3}$$

$$(1 + r)E_{annual} = (1 + p)E_{day}(1 + q)L_{ice-free} = (1 + p + q + pq)E_{day}L_{ice-free} \tag{4}$$

The term pq, is the increased rate caused by the interaction of daily mean evaporation and length of ice-free period. Normally, it is a second order term and can be ignored. Compared with 2014, the annual total evaporation at WBL increased by about 40% in 2015, while the daily mean evaporation increased by about 10%, and the length of ice-free period increased by about 25%. Therefore, the ice-free period contributed about 60% to the increase in the annual evaporation.

Given a typical daily mean evaporation rate of 2.6 mm day^{-1} and a

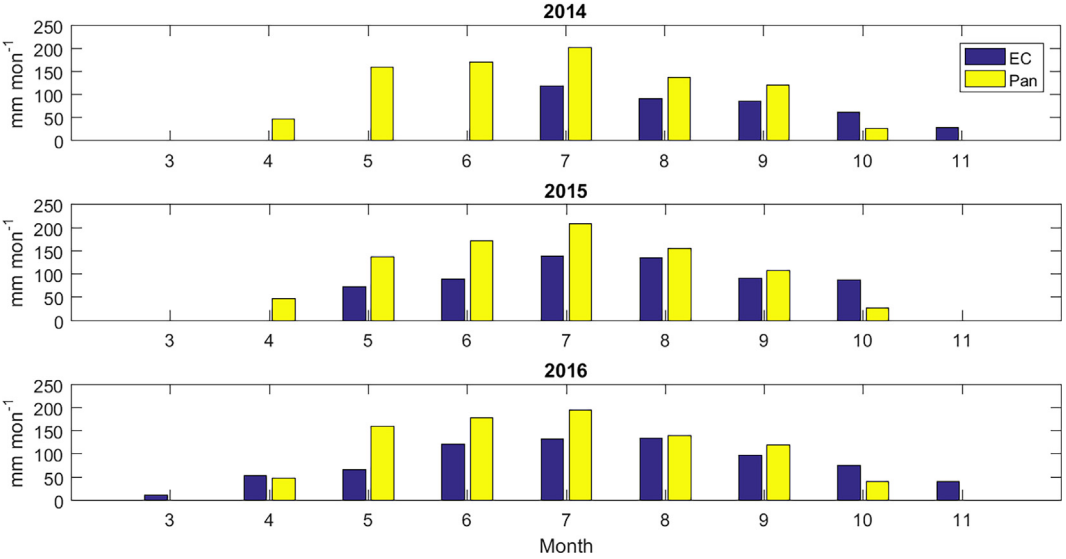

Fig. 9. Comparison of monthly evaporation measured at White Bear Lake with Class A pan evaporation.

length of ice-free period of 250 days, a 1% error represent a 0.026 mm day^{-1} in the daily mean evaporation and 2.5 days in the length of ice-free period. Without accurate in-situ record of ice phenology of a lake, it is very likely to have a 2.5-day error in the length of ice-free period.

5.1.2. Lake evaporation and pan evaporation

Fig. 9 shows the comparison between monthly evaporation at WBL and the evaporation from a Class A evaporation pan 18 km away from WBL on the St Paul campus at the University of Minnesota. The evaporation measured by EC at WBL was greatest in July and August, and the fall evaporation was more active than spring (i.e. the shape of the distribution was unimodal and left-skewed). The pan evaporation was greatest in July while the spring evaporation was larger than fall (i.e. unimodal but right-skewed), and it exhibited a larger seasonal variability compared to the lake. These patterns indicate that the pan evaporation was mainly driven by variability in solar radiation. The lake-to-pan evaporation ratio showed large monthly and inter-annual variability. For example, the ratio increased from 0.5 to 0.9 from May to September, and the ratio was larger than 1 in April and October. The August ratio varied between 0.66 and 0.96 for the three years. The annual total pan evaporation was 864 mm, 853 mm, and 877 mm from 2014 to 2016, respectively. These values were considerably larger than the gap-filled EC measurements and showed relatively little inter-annual variability. The lake-to-pan evaporation ratio for the annual total was 0.65, 0.91 and 0.87 for these three years, respectively. These analyses demonstrate that it is difficult to derive a single coefficient between annual pan evaporation and WBL evaporation. It should be noted that the variability in the length of the ice-free period can have a nonlinear effect on these ratios making it impractical to obtain a representative annual value for a temperate lake.

5.2. Retrospective evaporation

In the past 40 years, WBL has experienced two significant water level declines: 1986 to 1990 and 2003 to 2012 (Fig. 8). Both periods coincided with years with less precipitation and greater evaporation than the average. Our residual analyses suggest that the flux of lake water entering groundwater was larger than the average over the same period. This indicates that the groundwater aquifer was also at relatively low levels due to the low precipitation. Further, while the entire region was in a drought during these periods, groundwater pumping was also estimated to be greater due to agricultural and municipal usage (Jones et al., 2013). For example, over the 10-year period 2003 to 2012, mean annual precipitation was 822 ± 83 mm year^{-1} (mean ± standard deviation); the modeled annual evaporation was 756 ± 79 mm; and the derived mean seepage to groundwater was 244 ± 132 mm year^{-1}. For regional context, we compared the modeled retrospective annual evaporation at WBL to our long-term EC measurements of evapotranspiration (ET) at corn/soybean sites in Rosemount, MN, at the southern edge of the Twin Cities Metropolitan Area (Baker and Griffis, 2005; Baker et al., 2012; Griffis et al., 2016). Over the same period (2003 to 2012) the mean annual ET was 522 ± 52 mm over croplands. The mean annual ET for corn and soybean systems were not statistically different, with mean annual values of 507 ± 53 mm and 534 ± 52 mm, respectively. Year 2003 and 2012 were two notable drought years within the region. The modeled lake evaporation for 2003 and 2012 was 723 mm and 917 mm, respectively, while the pan evaporation for these two years was 879 mm and 1031 mm, respectively. The annual ET from crops was about 100 mm lower than the 10-year average for corn/soybean with minimum values of 423 and 472 mm in 2003 and 2012, respectively. These relatively low ET rates highlight how declining soil water content and drought stress likely increased the demand for irrigation. It is likely that such drought periods have exacerbated groundwater usage and have contributed to the decline in groundwater and lake water level within the region (Jones et al., 2013).

5.3. Projected evaporation

Given that lake evaporation is affected by multiple atmospheric variables and processes, long-term trends in those variables are critical in determining the trend in daily evaporation rate and annual total evaporation. The forcing data under RCP8.5 scenario indicate that air temperature and humidity will rise, while wind speed will decrease (Fig. 8). Correspondingly, the lake water surface temperature is expected to enhance the vertical vapor pressure gradient. These recent regional trends are consistent with the observed global trends over the past decades (Willett et al., 2008; McVicar et al., 2012; O'Reilly, et al., 2015). Although the projected modeling results indicate that the effects of changes in wind speed, vapor pressure difference and net radiation might be compensatory with respect to their influence on the daily mean evaporation rate, the change in length of the ice-free period will be a major factor driving increases in the annual total evaporation. The relation between evaporation and ice phenology deserves more research to understand the feedback processes and the potential amount

of inter-annual variability in evaporation from temperate closed-basin lakes.

We note that wind speed forcing data has opposite trends in the retrospective modeling and the projected modeling. These trends are consistent with previous studies (Holt and Wang, 2012; Kulkarni and Huang, 2014; Ashtine et al., 2016). The mechanism underlying these trends is largely driven by changes in the atmospheric circulation and require further investigation. Hobbins et al. (2012) found that the most important drivers of the atmospheric evaporative demand for our study area were air temperature, specific humidity, downwelling shortwave radiation, downwelling longwave radiation and wind speed. This indicates that compared with the wind speed, the vapor pressure difference at the lake surface, which is mainly influenced by both air temperature and specific humidity, is more critical in affecting the daily lake evaporation rate in the region.

The projected modeling results indicate that increasing rate of evaporation is likely to outpace changes in precipitation. It is estimated that annual evaporation at WBL will increase by 1.4 (mm year^{-1}) year^{-1} ($p < 0.01$) over this century, while the annual precipitation is expected to increase by about 1.1 (mm year^{-1}) year^{-1} ($p = 0.06$). Furthermore, there will be increasing probability of more extreme large evaporation years compared with current climate status. Overall, we expect decreases in the moving average of WBL lake water level and increases in lake level variability.

5.4. Regional implications

The Mississippi River – Twin Cities watershed has more than 1.8 million people and over 250 lakes (Anderson, et al., 2013). Many of these lakes have shown high sensitivity to variations in climate and water use. Our observations and model analyses support that lake levels within the region are closely coupled to evaporation and that future scenarios show a tendency for increased likelihood of lower water levels and more extreme fluctuations in lake levels. Unfortunately, detailed observations and modeling for such lakes remains rare, and therefore, their utility in effectively managing these water resources remains limited. There is an increasing need for developing comprehensive water management strategies to address the potential impacts of extreme climate events and climate change in light of increasing population and growing demand for these water resources. Understanding and forecasting changes in the magnitude of evaporation cannot be ignored. For WBL, the water loss from a typical evaporation rate of 5 mm per day during the summer is equivalent to 4.9×10^4 m^3 of water or roughly 0.5 m^3 s^{-1} of continuous 24-h pumping. An advanced ice-out date or postponed ice-in date of just one day is likely to result in an additional water loss of 2×10^4 m^3. Thus, small changes in the evaporation rate or ice phenology can have significant impacts on available water for these communities. Proposed water augmentation strategies that are designed to compensate for declining lake levels within the region for the present climate must be aware of the potential changes in supply and demand as climate continues to warm. Further, according to recent data from the USGS, per capita water use in Minnesota is about 0.23 m^3 per day (Maupin et al., 2010). The additional 100 mm of evaporation at WBL resulting from the long-term change in climate is equivalent to the annual water use of over 11,000 people and further highlights the need for sound water use management strategies. The combination of long-term evaporation measurements and modeling for sentinel lakes should be adopted as a strategy to help protect lakes and the ecosystem services that they provide.

The annual changes in water level of WBL showed strong coherence to changes in the regional lake water levels from 1925 to 2016 (Fig. 10). The changes in WBL water level and the median changes in the regional lake water levels exhibited very similar statistical characteristics including the overall sign. They were also significantly correlated with a coefficient of 0.68 ($p < 0.01$). As a closed-basin lake, WBL also showed a larger variation in the water level than the regional median value, but the water level changes of WBL were usually within the ranges bounded by the whiskers of the box plot. Such coherence implies that the regional lake water levels were collectively impacted by the large scale synoptic and climatic drivers influencing the regional precipitation and evaporation. Previous studies have shown that decadal changes in water levels of closed-basin lakes in North America were correlated to large scale climate teleconnections such as the Atlantic Multidecadal Oscillation (AMO) and the North Atlantic Oscillation (NAO) (Hanrahan et al., 2010; Hanrahan et al., 2014; Watras et al., 2014). These teleconnections can help us further understand the inter-annual relationship between climate and regional water balance. For example, previous research has shown that the 2009/2010 El Niño winter induced higher-than-normal air temperature in North America and mild ice conditions over the Great Lakes (Bai et al., 2011). In our study period, the increases in mean annual air temperature and precipitation from 2014 to 2016 in the Twin Cities and the changes in their patterns were potentially related to a phase shift in the El Niño–Southern Oscillation (ENSO) from a neutral to El Niño state. Correspondingly, we observed a relative longer ice-free season and larger annual evaporation at WBL in 2015 and 2016 than 2014. Thus, long-term projections of lake evaporation will also be influenced by the frequency and persistence of large scale atmospheric circulations. However, the influence of climate change on such teleconnections is poorly understood (Hanrahan et al., 2010). Therefore, more observations and modeling studies are needed to improve our understanding of these factors.

6. Conclusion

(1) Daily evaporation at WBL was strongly influenced by synoptic-scale variability. The heat released from the lake was the main energy source for evaporation in the fall. The annual evaporation at WBL from 2014 to 2016 was 559 ± 22 mm, 779 ± 81 mm, and 766 ± 11 mm, respectively. The annual evaporation in 2014 was least among the three years, due to its relatively short ice-free period and its relatively lower daily evaporation rate.

(2) The retrospective analyses indicated that WBL annual total evaporation increased by about 3.8 mm year^{-1} from 1979 to 2016, which was attributed to increased daily mean evaporation during the ice-free period. The increase of daily mean evaporation was driven by the increased wind speed and lake-surface vapor pressure gradient. The lake level declines at WBL during 1986–1990 and 2003–2012 were caused by the coupled low precipitation and high evaporation. This finding implies that a regional drought and potential intensified groundwater use can have a dramatic impact on water level at a closed-basin lake.

(3) Model results suggest that annual evaporation at WBL will increase 1.4 mm year^{-1} over this century under the RCP 8.5 scenario, which is largely driven by the extended ice-free periods. At the end of this century, the ice-cover period will shorten by more than a month, and the annual evaporation will increase by an equivalent 9.8×10^5 m^3 of water.

(4) Our observations and model analyses support that lake levels within the region are closely coupled to evaporation. Lake evaporation is expected to increase due to the extended ice-free period as climate continues to warm. A tendency for increased likelihood of lower water levels and greater fluctuations in water level for WBL and other lakes within the region is expected.

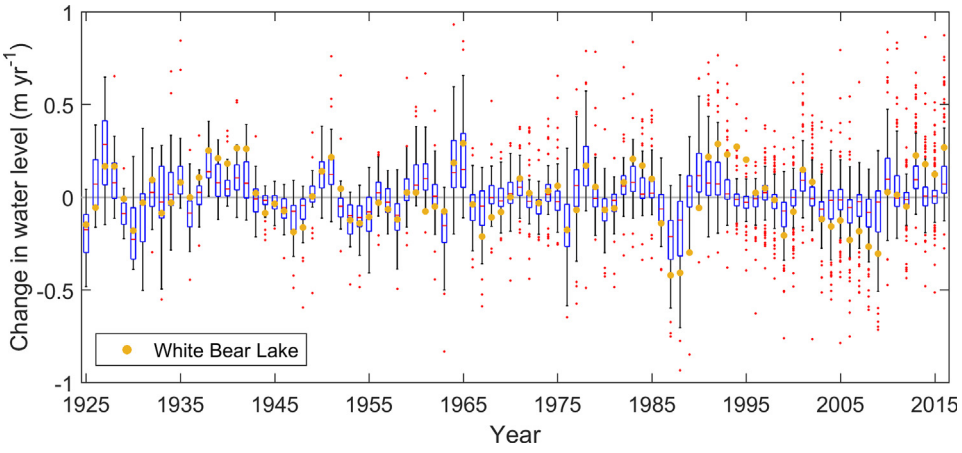

Fig. 10. Box-and-whisker plot of the annual changes in water level of lakes in the Twin Cities Metropolitan region from 1925 to 2016. The lake water levels were retrieved from MNDNR website. The changes in water level are the central differences of the annual mean water levels. The filled circles represent the changes in water level of White Bear Lake. Following the 1980 s there are more available observations (Fig. S8) and there is an increase in the number of outliers shown in the box plot. The water level changes of White Bear Lake fall outside of the quantiles more frequently.

Acknowledgements

We acknowledge the Nicholson family and the Becker family for allowing us to access White Bear Lake through their private property. Financial support and scientific instruments were provided by AmeriFlux, the Minnesota Corn Research and Promotion Council [grant number 4101-15SP] and the Minnesota DNR. USDA-ARS provided maintenance and logistical support for this project. Finally, we acknowledge the White Bear Lake Conservation District for their interest and continued support. We express our since thanks to Editor Tim R. McVicar, Associate Editor Joshua Larsen, and two reviewers, Peter Blanken (University of Colorado, Boulder, Colorado, United States) and one anonymous reviewer, for their helpful comments and suggestions. All data from this study will be made available at https://www.biometeorology.umn.edu/research/data-archives.

Appendix A. Supplementary data

Supplementary data associated with this article can be found, in the online version, at http://dx.doi.org/10.1016/j.jhydrol.2018.03.059.

References

Adrian, R., O'Reilly, C.M., Zagarese, H., Baines, S.B., Hessen, D.O., Keller, W., Livingstone, D.M., Sommaruga, R., Straile, D., Van Donk, E., Weyhenmeyer, G.A., Winder, M., 2009. Lakes as sentinels of climate change. Limnol. Oceanogr. 54, 2283–2297. http://dx.doi.org/10.4319/lo.2009.54.6_part_2.2283.

Almendinger, J.E., 1990. Groundwater control of closed-basin lake levels under steady-state conditions. J. Hydrol. 112, 293–318. http://dx.doi.org/10.1016/0022-1694(90)90020-X.

Anderson, P., Christopherson, D., Duffey, D., Genet, J., Monson, B., 2013. Mississippi River-Twin Cities Watershed Monitoring and Assessment Report, Minnesota Pollution Control Agency. Available at < https://www.pca.state.mn.us/sites/default/files/wq-ws3-07010206b.pdf > .

Ashtine, M., Bello, R., Higuchi, K., 2016. Assessment of wind energy potential over Ontario and Great Lakes using the NARR data: 1980–2012. Renewable Sustainable Energy Rev. 56, 272–282. http://dx.doi.org/10.1016/j.rser.2015.11.019.

Ayenew, T., Becht, R., 2008. Comparative assessment of the water balance and hydrology of selected Ethiopian and Kenyan Rift Lakes, pp. 181–196. < http://dx.doi.org/10.1111/j.1440-1770.2008.00368.x > .

Bai, X., Wang, J., Liu, Q., Wang, D., Liu, Y., 2011. Severe ice conditions in the Bohai Sea, China, and mild ice conditions in the great lakes during the 2009/10 winter: Links to el niño and a strong negative Arctic Oscillation. J. Appl. Meteorol. Climatol. 50, 1922–1935. http://dx.doi.org/10.1175/2011JAMC2675.1.

Baker, J.M., Griffis, T.J., 2005. Examining strategies to improve the carbon balance of corn/soybean agriculture using eddy covariance and mass balance techniques. Agric. For. Meteorol. 128, 163–177. http://dx.doi.org/10.1016/j.agrformet.2004.11.005.

Baker, J.M., Griffis, T.J., Ochsner, T.E., 2012. Coupling landscape water storage and supplemental irrigation to increase productivity and improve environmental stewardship in the U.S. Midwest. Water Resour. Res. 48, 1–12. http://dx.doi.org/10.1029/2011WR011780.

Blanken, P.D., Rouse, W.R., Culf, A.D., Spence, C., Boudreau, L.D., Jasper, J.N., Kochtubajda, B., Schertzer, W.M., Marsh, P., Verseghy, D., 2000. Eddy covariance measurements of evaporation from Great Slave Lake, Northwest Territories. Canada. Water Resour. Res. 36, 1069–1077. http://dx.doi.org/10.1029/1999WR900338.

Blanken, P.D., Spence, C., Hedstrom, N., Lenters, J.D., 2011. Evaporation from Lake Superior: 1. Physical controls and processes. J. Great Lakes Res. 37, 707–716. http://dx.doi.org/10.1016/j.jglr.2011.08.009.

Boyd, C.E., 2015. Particulate matter color, turbidity, and light. In: Water Quality: An Introduction, pp. 101–112.

Brustaert, W., 1982. Chapter 11 – mass budget methods. In: Evaporation into the Atmosphere-Theory, History and Application. D. Reidel pub. Comp, Dordrecht-Boston-London, pp. 231–262.

Demuth, H., Beale, M., Jess, O. De, Hagan, M., 2014. Neural network design. Martin Hagan.

Deng, B., Liu, S., Xiao, W., Wang, W., Jin, J., Lee, X., 2013. Evaluation of the CLM4 lake model at a large and shallow freshwater lake. J. Hydrometeorol. 14, 636–649. http://dx.doi.org/10.1175/JHM-D-12-067.1.

Dunne, J.P., John, J.G., Adcroft, A.J., Griffies, S.M., Hallberg, R.W., Shevliakova, E., Stouffer, R.J., Cooke, W., Dunne, K.A., Harrison, M.J., Krasting, J.P., 2012. GFDL's ESM2 global coupled climate-carbon earth system models. Part I: physical formulation and baseline simulation characteristics. J. Clim. 25, 6646–6665. http://dx.doi.org/10.1175/JCLI-D-11-00560.1.

Fang, X., Stefan, H.G., 1996. Long-term lake water temperature and ice cover simulations/measurements. Cold Reg. Sci. Technol. 24, 289–304. http://dx.doi.org/10.1016/0165-232X(95)00019-8.

Friedl, M.A., Sulla-Menashe, D., Tan, B., Schneider, A., Ramankutty, N., Sibley, A., Huang, X., 2010. MODIS Collection 5 global land cover: algorithm refinements and characterization of new datasets. Remote Sens. Environ. 114, 168–182. http://dx.doi.org/10.1016/j.rse.2009.08.016.

Friedrich, K., Grossman, R.L., Huntington, J., Blanken, P.D., Lenters, J., Holman, K.L.D., Gochis, D., Livneh, B., Prairie, J., Skeie, E., Healey, N.C., Dahm, K., Pearson, C., Finnessey, T., Hook, S.J., KowaLsKi, T., 2018. Reservoir evaporation in the Western United States. Bull. Am. Meteorol. Soc. 99, 167–187. http://dx.doi.org/10.1175/BAMS-D-15-00224.1.

Fritscht, F.N., Carlson, R.E., 1980. Monotone piecewise cubic interpolation. SIAM J. Numer. Anal. 17. http://dx.doi.org/10.1137/0717021.

Gianniou, S.K., Antonopoulos, V.Z., 2007. Evaporation and energy budget in Lake Vegoritis. Greece. J. Hydrol. 345, 212–223. http://dx.doi.org/10.1016/j.jhydrol.2007.08.007.

Granger, R.J., Hedstrom, N., 2011. Modelling hourly rates of evaporation from small lakes. Hydrol. Earth Syst. Sci. 15, 267–277. http://dx.doi.org/10.5194/hess-15-267-2011.

Griffis, T.J., Wood, J.D., Baker, J.M., Lee, X., Xiao, K., Chen, Z., Welp, L.R., Schultz, N.M., Gorski, G., Chen, M., Nieber, J., 2016. Investigating the source, transport, and isotope composition of water vapor in the planetary boundary layer. Atmos. Chem. Phys. 16, 5139–5157. http://dx.doi.org/10.5194/acp-16-5139-2016.

Gronewold, A.D., Anderson, E.J., Lofgren, B., Blanken, P.D., Wang, J., Smith, J., Hunter, T., 2015. Impacts of extreme 2013–2014 winter conditions on Lake Michigan's fall heat content, surface temperature. Geophys. Res. Lett. 3364–3370. http://dx.doi.org/10.1002/2015GL063799.

Hanrahan, J., Roebber, P., Kravtsov, S., 2014. Attribution of decadal-scale lake-level trends in the Michigan-Huron system. Water (Switzerland) 6, 2278–2299. http://dx.doi.org/10.3390/w6082278.

Hanrahan, J.L., Kravtsov, S.V., Roebber, P.J., 2010. Connecting past and present climate variability to the water levels of Lakes Michigan and Huron. Geophys. Res. Lett. 37, 1–6. http://dx.doi.org/10.1029/2009GL041707.

Henderson-Sellers, B., 1985. New formulation of eddy diffusion thermocline models. Appl. Math. Model. 9, 441–446. http://dx.doi.org/10.1016/0307-904X(85)90110-6.

Hobbins, M., Wood, A., Streubel, D., Werner, K., 2012. What drives the variability of evaporative demand across the conterminous United States? J. Hydrometeorol. 13, 1195–1214. http://dx.doi.org/10.1175/JHM-D-11-0101.1.

Holt, E., Wang, J., 2012. Trends in wind speed at wind turbine height of 80 m over the contiguous United States using the north American Regional Reanalysis (NARR). J. Appl. Meteorol. Climatol. 51, 2188–2202. http://dx.doi.org/10.1175/JAMC D 11 0205.1.

Hu, C., Wang, Y., Wang, W., Liu, S., Piao, M., Xiao, W., Lee, X., 2017. Trends in evaporation of a large subtropical lake. Theor. Appl. Climatol. 1–12. http://dx.doi.org/10.1007/s00704-016-1768-z.

Huybers, K., Rupper, S., Roe, G.H., 2016. Response of closed basin lakes to interannual climate variability. Clim. Dyn. 46, 3709–3723. http://dx.doi.org/10.1007/s00382-015-2798-4.

Irish, R.R., 2000. Landsat 7 automatic cloud cover assessment. AeroSense 2000 (4049), 348–355. http://dx.doi.org/10.1117/12.410358.
Jones, P.M., Trost, J.J., Rosenberry, D.O., Jackson, P.R., Bode, J.A., and O'Grady, R.M., 2013. Groundwater and surface-water interactions near White Bear Lake, Minnesota, through 2011: U.S. Geological Survey Scientific Investigations Report 2013–5044, 73 p.
Jones, P.M., Trost, J.J., Diekoff, A.L., Rosenberry, D.O., White, E.A., Erickson, M.L., Morel, D.L., Heck, J.M., 2016. Statistical analysis of lake levels and field study of groundwater and surface-water exchanges in the northeast Twin Cities Metropolitan Area, Minnesota, 2002 through 2015: chapter A of water levels and groundwater and surface-water exchanges in lakes of the northeast Twin Cities Metropolitan Area, Minnesota, 2002 through 2015. US Geol. Surv. http://dx.doi.org/10.3133/sir20165139A.
Kirillin, G., Phillip, W., Engelhardt, C., Nützmann, G., 2013. Net groundwater inflow in an enclosed lake: from synoptic variations to climatic projections. Hydrol. Process. 27, 347–359. http://dx.doi.org/10.1002/hyp.9227.
Kulkarni, S., Huang, H.-P., 2014. Changes in surface wind speed over North America from CMIP5 model projections and implications for wind energy. Adv. Meteorol. 2014, 1–10. http://dx.doi.org/10.1155/2014/292768.
Lee, X., Massman, W., Law, B., 2004. Handbook of micrometeorology: a guide for surface flux measurement and analysis. Atmospheric and Oceanographic Sciences Library.
Legesse, D., Vallet-Coulomb, C., Gasse, F., 2004. Analysis of the hydrological response of a tropical terminal lake, Lake Abiyata (main Ethiopian rift valley) to changes in climate and human activities. Hydrol. Process. 18, 487–504. http://dx.doi.org/10.1002/hyp.1334.
Lenters, J.D., Kratz, T.K., Bowser, C.J., 2005. Effects of climate variability on lake evaporation: results from a long-term energy budget study of Sparkling Lake, northern Wisconsin (USA). J. Hydrol. 308, 168–195. http://dx.doi.org/10.1016/j.jhydrol.2004.10.028.
Li, X.-Y., Ma, Y.-J., Huang, Y.-M., Hu, X., Wu, X.-C., Wang, P., Li, G.-Y., Zhang, S.-Y., Wu, H.-W., Jiang, Z.-Y., Cui, B.-L., Liu, L., 2016. Evaporation and surface energy budget over the largest high-altitude saline lake on the Qinghai-Tibet Plateau. J. Geophys. Res. Atmos. 121, 10470–10485. http://dx.doi.org/10.1002/2016JD025027.
Li, X.Y., Xu, H.Y., Sun, Y.L., Zhang, D.S., Yang, Z.P., 2007. Lake-level change and water balance analysis at lake Qinghai, West China during recent decades. Water Resour. Manage. 21, 1505–1516. http://dx.doi.org/10.1007/s11269-006-9096-1.
Ma, N., Szilagyi, J., Niu, G.Y., Zhang, Y., Zhang, T., Wang, B., Wu, Y., 2016. Evaporation variability of Nam Co Lake in the Tibetan Plateau and its role in recent rapid lake expansion. J. Hydrol. 537, 27–35. http://dx.doi.org/10.1016/j.jhydrol.2016.03.030.
Maupin, M.A., Kenny, J.F., Hutson, S.S., Lovelace, J.K., Barber, N.L., Linsey, K.S., 2010. Estimated use of water in the United States in 2010. US Geol. Sur. http://dx.doi.org/10.3133/cir1405.
McComas, S., 2011. Aquatic Plant Point Intercept Survey for White Bear Lake, Washington County, Minnesota, 2011, White Bear Lake Conservation District. Available at < http://www.wblcd.org/pdf/reports/WBL%20report%20-%20avp%2011.pdf > .
McVicar, T.R., Roderick, M.L., Donohue, R.J., Li, L.T., Van Niel, T.G., Thomas, A., Grieser, J., Jhajharia, D., Himri, Y., Mahowald, N.M., Mescherskaya, A.V., Kruger, A.C., Rehman, S., Dinpashoh, Y., 2012. Global review and synthesis of trends in observed terrestrial near-surface wind speeds: implications for evaporation. J. Hydrol. 416–417, 182–205. http://dx.doi.org/10.1016/j.jhydrol.2011.10.024.
Minnesota Department of Natural Resources, 1998. Lake-ground water interaction study at White Bear Lake, Minnesota – Report to the Legislative Committee on Minnesota Resources. Available at < http://files.dnr.state.mn.us/publications/waters/wbl_98.pdf > .
Martínez, J.M.M., Alvarez, V.M., González-Real, M.M., Baille, A., 2006. A simulation model for predicting hourly pan evaporation from meteorological data. J. Hydrol. 318, 250–261. http://dx.doi.org/10.1016/j.jhydrol.2005.06.016.
Niedda, M., Pirastru, M., 2013. Hydrological processes of a closed catchment-lake system in a semi-arid Mediterranean environment. Hydrol. Process. 27, 3617–3626. http://dx.doi.org/10.1002/hyp.9478.
Nordbo, A., Launiainen, S., Mammarella, I., Leppäranta, M., Huotari, J., Ojala, A., Vesala, T., 2011. Long-term energy flux measurements and energy balance over a small boreal lake using eddy covariance technique. J. Geophys. Res. Atmos. 116, 1–17. http://dx.doi.org/10.1029/2010JD014542.
O'Reilly, et al., 2015. Rapid and highly variable warming of lake surface waters around the globe. Geophys. Res. Lett. 1–9. http://dx.doi.org/10.1002/2015GL066235.
Oleson, K.W., Lawrence, D.M., Bonan, G.B., Drewniak, B., Huang, M., Koven, C.D., Levis, S., Li, F., Riley, W.J., Subin, Z.M., Swenson, S.C., Thornton, P.E., Bozbiyik, A., Fisher, R., Heald, C.L., Kluzek, E., Lamarque, J.-F., Lawrence, P.J., Leung, L.R., Lipscomb, W., Muszala, S., Ricciuto, D.M., Sacks, W., Sun, Y., Tang, J., Yang, Z.-L., 2013. Technical Description of version 4.5 of the Community Land Model (CLM). < http://dx.doi.org/10.5065/D6RR1W7M > .
Papale, D., Reichstein, M., Aubinet, M., Canfora, E., Bernhofer, C., Kutsch, W., Longdoz, B., Rambal, S., Valentini, R., Vesala, T., Yakir, D., 2006. Towards a standardized processing of Net Ecosystem Exchange measured with eddy covariance technique: algorithms and uncertainty estimation. Biogeosciences 3, 571–583. http://dx.doi.org/10.5194/bg-3-571-2006.
Riahi, K., Rao, S., Krey, V., Cho, C., Chirkov, V., Fischer, G., Kindermann, G., Nakicenovic, N., Rafaj, P., 2011. RCP 8.5-A scenario of comparatively high greenhouse gas emissions. Clim. Change 109, 33–57. http://dx.doi.org/10.1007/s10584-011-0149-y.
Roderick, M.L., Rotstayn, L.D., Farquhar, G.D., Hobbins, M.T., 2007. On the attribution of changing pan evaporation. Geophys. Res. Lett. 34, 1–6. http://dx.doi.org/10.1029/2007GL031166.
Rouse, W.R., Blanken, P.D., Bussières, N., Walker, A.E., Oswald, C.J., Schertzer, W.M., Spence, C., 2008. An investigation of the thermal and energy balance regimes of great slave and great bear lakes. J. Hydrometeorol. 9, 1318–1333. http://dx.doi.org/10.1175/2008JHM977.1.
Santer, B.D., Mears, C., Wentz, F.J., Taylor, K.E., Gleckler, P.J., Wigley, T.M.L., Barnett, T.P., Boyle, J.S., Brüggemann, W., Gillett, N.P., Klein, S.A., Meehl, G.A., Nozawa, T., Pierce, D.W., Stott, P.A., Washington, W.M., Wehner, M.F., 2007. Identification of human-induced changes in atmospheric moisture content. Proc. Natl. Acad. Sci. U.S.A. 104, 15248–15253. http://dx.doi.org/10.1073/pnas.0702872104.
Schindler, D.W., 2009. Lakes as sentinels and integrators for the effects of climate change on watersheds, airsheds, and landscapes. Limnol. Oceanogr. 54, 2349–2358. http://dx.doi.org/10.4319/lo.2009.54.6_part_2.2349.
Shanahan, T.M., Overpeck, J.T., Sharp, W.E., Scholz, C.A., Arko, J.A., 2007. Simulating the response of a closed-basin lake to recent climate changes in tropical West Africa (Lake Bosumtwi, Ghana). Hydrol. Process. 21, 1678–1691. http://dx.doi.org/10.1002/hyp.6359.
Singh, V., Xu, C., 1997. Evaluation and generalization of 13 mass-transfer equations for determining free water evaporation. Hydrol. Process. 11, 311–323. http://dx.doi.org/10.1002/(SICI)1099-1085(19970315)11:3<311::AID-HYP446>3.3.CO;2-P.
Spence, C., Blanken, P.D., Lenters, J.D., Hedstrom, N., 2013. The importance of spring and autumn atmospheric conditions for the evaporation regime of lake superior. J. Hydrometeorol. 14, 1647–1658. http://dx.doi.org/10.1175/JHM-D-12-0170.1.
Stepanenko, V., Jöhnk, K.D., Machulskaya, E., Perroud, M., Subin, Z., Nordbo, A., Mammarella, I., Mironov, D., 2014. Simulation of surface energy fluxes and stratification of a small boreal lake by a set of one-dimensional models. Tellus, Ser. A Dyn. Meteorol. Oceanogr. 66. http://dx.doi.org/10.3402/tellusa.v66.21389.
Sturrock, A.M., Winter, T.C., Rosenberry, D.O., 1992. Energy budget evaporation from Williams Lake: a closed lake in north central Minnesota. Water Resour. Res. 28, 1605–1617. http://dx.doi.org/10.1029/92WR00553.
Subin, Z.M., Riley, W.J., Mironov, D., 2012. An improved lake model for climate simulations: model structure, evaluation, and sensitivity analyses in CESM1. J. Adv. Model. Earth Syst. 4, 1–27. http://dx.doi.org/10.1029/2011MS000072.
Tanner, B.D., Swiatek, E., Greene, J.P., 1993. Density fluctuations and use of the krypton hygrometer in surface flux measurements. Manage. Irrig. Drain. Syst. Integr. Perspect. Am. Soc. Civ. Eng. New York, NY 44, 945–952.
Trenberth, K.E., Asrar, G.R., 2014. Challenges and opportunities in water cycle research: WCRP contributions. Surv. Geophys. 35, 515–532. http://dx.doi.org/10.1007/s10712-012-9214-y.
Vainu, M., Terasmaa, J., 2014. Changes in climate, catchment vegetation and hydrogeology as the causes of dramatic lake-level fluctuations in the Kurtna Lake District, NE Estonia. Est. J. Earth Sci. 63, 45. http://dx.doi.org/10.3176/earth.2014.04.
Vallet-Coulomb, C., Legesse, D., Gasse, F., Travi, Y., Chernet, T., 2001. Lake evaporation estimates in tropical Africa (Lake Ziway, Ethiopia). J. Hydrol. 245, 1–18. http://dx.doi.org/10.1016/S0022-1694(01)00341-9.
van der Kamp, G., Keir, D., Evans, M.S., 2008. Long-term water level changes in closed-basin lakes of the Canadian prairies. Can. Water Resour. J. 33, 23–38. http://dx.doi.org/10.4296/cwrj3301023.
Vermote, E., 2015. MYD09A1 MODIS/Aqua Surface Reflectance 8-Day L3 Global 500m SIN Grid V006. < http://dx.doi.org/10.5067/MODIS/MYD09A1.006 > .
Vermote, E., Wolfe, R., 2015. MOD09GA MODIS/Terra Surface Reflectance Daily L2G Global 1kmand 500m SIN Grid V006. < http://dx.doi.org/10.5067/MODIS/MOD09GA.006 > .
Wang, B., Ma, Y., Ma, W., Su, Z., 2017. Physical controls on half-hourly, daily, and monthly turbulent flux and energy budget over a high-altitude small lake on the Tibetan Plateau. J. Geophys. Res. 122, 2289–2303. http://dx.doi.org/10.1002/2016JD026109.
Wang, W., Xiao, W., Cao, C., Gao, Z., Hu, Z., Liu, S., Shen, S., Wang, L., Xiao, Q., Xu, J., Yang, D., Lee, X., 2014. Temporal and spatial variations in radiation and energy balance across a large freshwater lake in China. J. Hydrol. 511, 811–824. http://dx.doi.org/10.1016/j.jhydrol.2014.02.012.
Watras, C.J., Read, J.S., Holman, K.D., Liu, Z., Song, Y.-Y., Watras, A.J., Morgan, S., Stanley, E.H., 2014. Decadal oscillation of lakes and aquifers in the upper Great Lakes region of North America: hydroclimatic implications. Geophys Res Lett 41, 456–462. http://dx.doi.org/10.1002/2013GL058679.
Webb, E., Leuning, R., 1980. Correction of flux measurements for density effects due to heat and water vapour transfer. Q. J. Meteorol. Soc. 106, 85–100. http://dx.doi.org/10.1002/qj.49710644707.
Wild M. 2009. Global dimming and brightening: a review. Journal of Geophysical Research-Atmospheres 114: D00D16. < http://dx.doi.org/10.1029/2008JD011470 > .
Willett, K.M., Jones, P.D., Gillett, N.P., Thorne, P.W., 2008. Recent changes in surface humidity: Development of the HadCRUH dataset. J. Clim. 21, 5364–5383. http://dx.doi.org/10.1175/2008JCLI2274.1.
Wilson, K., Goldstein, A., Falge, E., Aubinet, M., Baldocchi, D., Berbigier, P., Bernhofer, C., Ceulemans, R., Dolman, H., Field, C., Grelle, A., Ibrom, A., Law, B.E., Kowalski, A., Meyers, T., Moncrieff, J., Monson, R., Oechel, W., Tenhunen, J., Valentini, R., Verma, S., 2002. Energy balance closure at FLUXNET sites. Agric. For. Meteorol. 113, 223–243. http://dx.doi.org/10.1016/S0168-1923(02)00109-0.
Winter, T.C., 1995. Hydrological processes and the water budget of lakes. In: Physics and Chemistry of Lakes, pp. 37–62. http://dx.doi.org/10.1007/978-3-642-85132-2_2.
Xia, Y., Mitchell, K., Ek, M., Sheffield, J., Cosgrove, B., Wood, E., Luo, L., Alonge, C., Wei, H., Meng, J., Livneh, B., Lettenmaier, D., Koren, V., Duan, Q., Mo, K., Fan, Y., Mocko, D., 2012. Continental-scale water and energy flux analysis and validation for the North American Land Data Assimilation System project phase 2 (NLDAS-2): 1. Intercomparison and application of model products. J. Geophys. Res. 117, D03109. http://dx.doi.org/10.1029/2011jd016048.
Zhang, B., Wu, Y., Zhu, L., Wang, J., Li, J., Chen, D., 2011. Estimation and trend detection of water storage at Nam Co Lake, central Tibetan Plateau. J. Hydrol. 405, 161–170. http://dx.doi.org/10.1016/j.jhydrol.2011.05.018.